Journal of Volcanology and Geothermal Research 186 (2009) 331–348

Contents lists available at ScienceDirect

Journal of Volcanology and Geothermal Research

journal homepage: www.elsevier.com/locate/jvolgeores

Lava shields and fissure eruptions of the Western Volcanic Zone, Iceland: Evidence for magma chambers and crustal interaction

Deborah E. Eason *, John M. Sinton

Department of Geology and Geophysics, School of Ocean and Earth Science and Technology, 1680 East–West Road, University of Hawaii, Honolulu, HI 96822, United States

ARTICLE INFO

Article history:
Received 19 December 2008
Accepted 30 June 2009
Available online 5 July 2009

Keywords:
Iceland
mid-ocean ridge
magma chambers
crustal interaction
MORB
igneous petrology

ABSTRACT

Volcanic eruptions in Iceland occur either from fissures or central vents (lava shields). Within the post-glacial Western Volcanic Zone, the Thjófahraun fissure-fed lava field and Lambahraun lava shield were both erupted ~4000 yrs B.P. with eruptive centers separated by only ~25 km. Thjófahraun erupted ~1 km^3 of pāhoehoe and 'a'ā lava from a 9-km long fissure, whereas the Lambahraun lava shield erupted >7 km^3 of low effusion-rate pāhoehoe. Thjófahraun lavas contain higher K, Rb, Y and Zr, and lower CaO than Lambahraun lavas at the same MgO, with variations broadly consistent with evolution by low-pressure crystal fractionation. Lambahraun spans a larger range of MgO, which generally decreases over time during the eruption. Lambahraun samples with high Al_2O_3 and low TiO_2 and FeO likely reflect up to 15% plagioclase accumulation. In addition, all samples from Lambahraun exhibit increasing CaO and Nb/Zr with decreasing MgO and overall incompatible-element enrichments greater than predicted by crystal fractionation alone. Although the increase in Nb/Zr and other incompatible elements could be explained by gradually more incompatible-element enriched parental magma being supplied to the magmatic system during the course of the Lambahraun eruption, this process requires very small-scale trace element heterogeneities in the mantle that are apparently decoupled from isotopic variations and a systematic relationship between parental magma composition and extent of differentiation. Alternatively, correlations among incompatible element concentration, increasing differentiation and time during the eruption can be related by concurrent wallrock assimilation and crystallization during melt migration through the crust. Geochemical modeling of assimilation of wallrock clinopyroxene concurrent with crystallization of olivine (±plagioclase) effectively reproduces the observed chemical variations of Lambahraun samples. Similar chemical characteristics exist in several other Western Volcanic Zone lava shields but not in fissure eruptions. Magmas that fed fissure eruptions may also have been modified by interaction with the crust prior to aggregation in crustal magma chambers, but the geochemical signature of this process is obscured by magma mixing. In contrast, Icelandic lava shields that preserve deeper level processes may not have developed shallow magma chambers; rather they probably represent slow effusion from magma systems that are continually being recharged and reacting with the crust during the course of their eruptions.

1. Introduction

The study of the products of single volcanic eruptions is one of the most direct ways to assess the nature of underlying magmatic processes that occur prior to and during eruptions. Erupted volumes and chemical composition of individual lava flows constrain the size, temperature, and internal variation within sub-volcanic magma reservoirs, which in turn can affect the style of eruption. The nature and extent of chemical heterogeneity within individual eruptive episodes can be used to constrain melting, differentiation and mixing that must occur over time scales limited by eruption durations and periods between eruptions at specific locations. Among the questions that can be addressed by such studies include magmatic controls on eruption rate, resultant lava morphology, and the nature of magma chambers, if any, from which the magma is erupted.

To fully address relationships among melting and differentiation processes of individual eruptions and their corresponding eruptive style, magma supply, and crustal storage characteristics requires information on flow morphology, eruptive vent characteristics, estimates of erupted volume, and sufficient sampling to quantify chemical heterogeneity. The highest level of detail for volcanic eruptions can only be attained for historical events with contemporaneous observations and sampling. For pre-historical eruptions, detailed mapping and sampling is especially difficult to accomplish along submarine mid-ocean ridges and consequently, studies at the scale of individual mid-ocean ridge eruption units are rare (Perfit and Chadwick, 1998; Embley et al., 2000; Sinton et al., 2002; Bergmanis et al., 2007). Even in Iceland, where the mid-ocean ridge system is well exposed above sea level, there have been relatively few detailed studies of single lava flow

* Corresponding author. Tel.: +1 808 956 9544.
E-mail addresses: deborahe@hawaii.edu (D.E. Eason), sinton@hawaii.edu (J.M. Sinton).

0377-0273/$ – see front matter © 2009 Elsevier B.V. All rights reserved.
doi:10.1016/j.jvolgeores.2009.06.009

fields (Maclennan et al., 2003b) and no lava shields have erupted in historical time.

The neovolcanic zones of Iceland are ideal for investigating processes associated with individual eruptive units. The very slow-spreading (3–7 mm/yr (LaFemina et al., 2005)) Western Volcanic Zone (WVZ) forms a 170-km long portion of the Mid-Atlantic Ridge plate boundary, comprising the western limb of a microplate in South Iceland (Fig. 1). All post-glacial (since ~12 ka) eruptive units of the WVZ have been mapped, sampled and analyzed for major and trace elements, and age constraints have been determined for most eruptions from ^{14}C-dating and tephrochronology (Sinton et al., 2005). Sr, Nd, Pb and Hf isotopic ratios have been determined for a subset of samples (Halldórsson et al., 2008b). Lava flow fields produced during single eruptive episodes range from ~0.1 to >15 km^3, encompassing a range in lava morphology and styles of eruptive activity. Thus, this portion of the ridge is an ideal location to investigate a variety of volcanic processes, including spatial and temporal variations in eruption style, melting and differentiation processes, and source heterogeneity.

Volcanic eruptions in Iceland occur either as fissure or central vent (lava shield) eruptions. Fissure eruptions tend to produce lavas indicative of high average effusion rates from small spatter cones extending over several kilometers to tens of kilometers. In contrast, most lava shields are composed almost entirely of relatively dense pāhoehoe lava from edifices that are surmounted by a central caldera, typically 0.5–2 km in diameter. However, the nature of the reservoirs that feed these eruptions and the underlying magmatic processes that occur prior to eruption are poorly known. Sinton et al. (2005) proposed that fissure eruptions tap extant, well-mixed crustal magma chambers, whereas the chemical variations in lava shields are inconsistent with large, well-mixed magma reservoirs and seem to require mantle recharge during the course of several decade-long eruptions. In order to better understand the underlying magmatic processes associated with differences in eruptive style, we have undertaken a detailed study of the products of two WVZ eruptions — a lava shield (Lambahraun) and a fissure eruption (Thjófahraun) — both erupted about 4000 yrs ago with the locus of activity separated by about 25 km (Fig. 2). The selection of two units erupted close to one another in both space and time along the WVZ minimizes temporal and spatial variations in processes related to mantle composition and crustal structure. We use the geochemical variability of the erupted products of Lambahraun and Thjófahraun to constrain the differences in their respective crustal reservoirs, their melting and differentiation histories, and potential source variations. The selection of Thjófahraun and Lambahraun requires that any spatial or temporal variations must be less than ~25 km and ~400 years.

2. Data and methods

2.1. Field study

The areal limits of both Lambahraun and Thjófahraun flow fields and internal contacts within the Thjófahraun field were determined using a combination of aerial photographs and field mapping; the

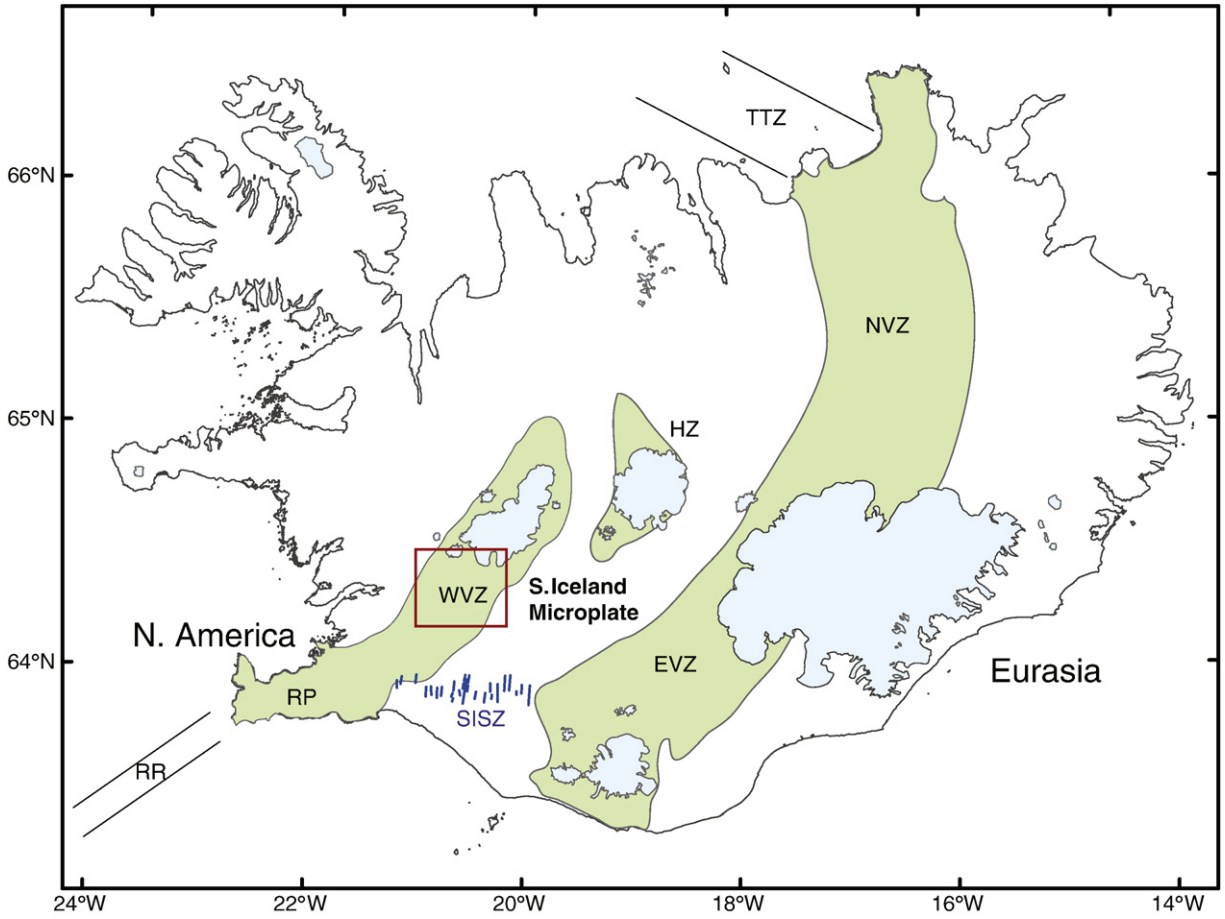

Fig. 1. Map of Iceland showing the principal plate-boundary zones in Iceland: the Northern Volcanic Zone (NVZ), Eastern Volcanic Zone (EVZ), Hofsjökull Zone (HZ), Western Volcanic Zone (WVZ), and Reykjanes Peninsula (RP). These volcanic zones connect up to the Tjörnes Transform Zone (TTZ) and Reykjanes Ridge (RR) offshore. The south Iceland seismic zone (SISZ) represents a transform boundary on the south side of the south Iceland microplate. Box outlines the area of Fig. 2.

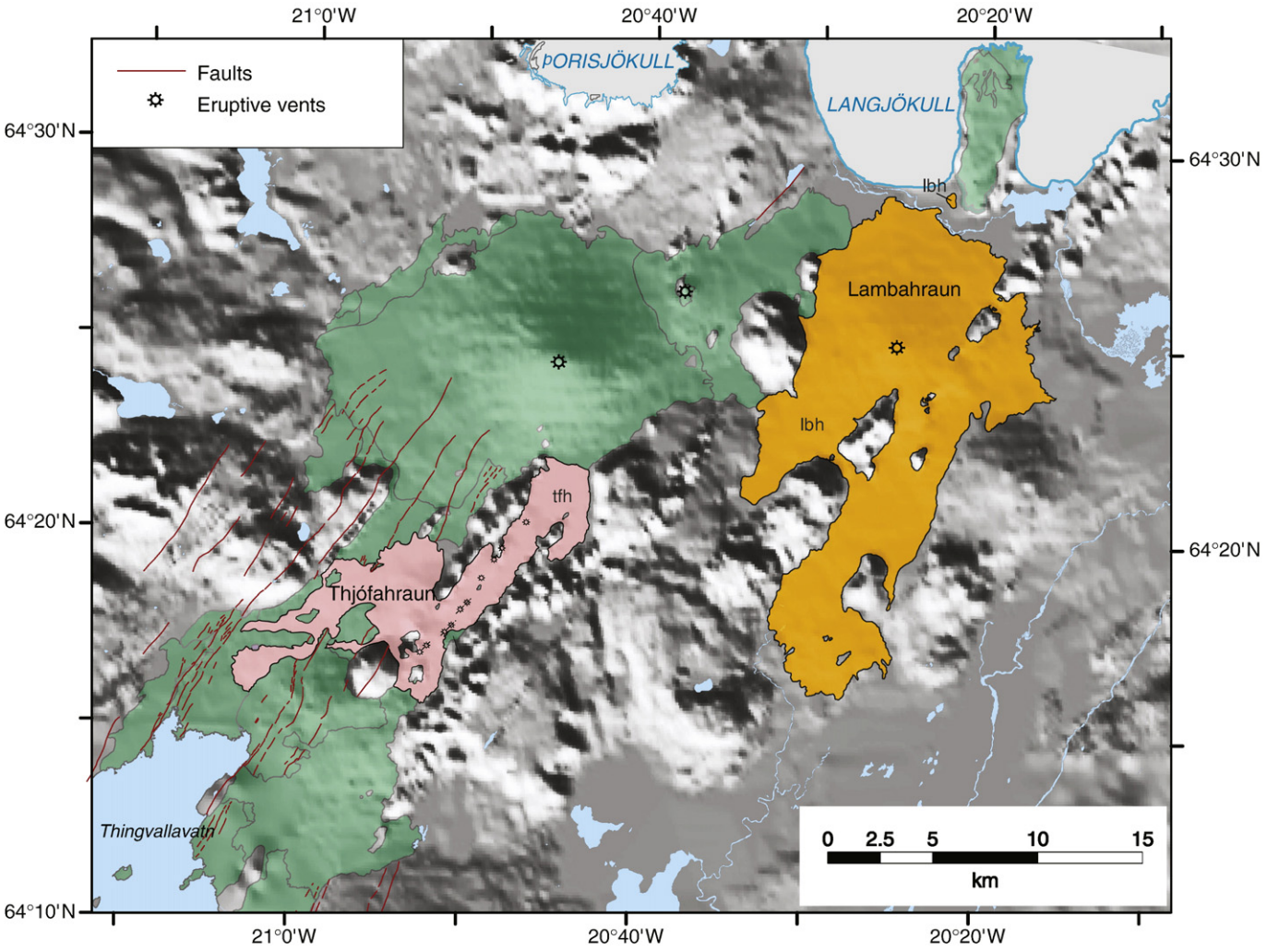

Fig. 2. Shaded relief map of the central Western Volcanic Zone showing the distribution of post-glacial lava units, including Lambahraun (lbh) and Thjófahraun (tfh). Modified after Sæmundsson (1992) and Sinton et al. (2005).

external contacts shown in Figs. 2–4 are modified slightly from those of Sinton et al. (2005). Sub-units within the Thjófahraun field and their relative ages were determined from aerial photographs and field observations. Where possible, we attempted to assign individual flow units to the vents from which they were erupted, although this is typically only possible for the youngest units. Sixteen additional samples collected for this study from both units supplement the 33 analyses reported by Sinton et al. (2005) to better cover the spatial range of each flow field.

2.2. XRF analysis

Whole rock X-ray fluorescence (XRF) data were measured on the University of Hawai'i Siemens 303AS XRF spectrometer using a Rh-target, end-window X-ray tube. Whole rocks were crushed in an alumina swing mill, and powders were analyzed for major elements on fused disks following methods similar to those of Norrish and Hutton (1977). Trace elements were analyzed on pressed powder pellets. Peak intensities for the trace elements were corrected for backgrounds, line interferences and matrix absorption using methods similar to those of Chappell (1992). Corrected intensities were calibrated against a wide range of natural rock standards. Accuracy and precision data for this system are reported in Sinton et al. (2005). New analytical data are reported in Table 1. All analytical data from Lambahraun and Thjófahraun, including previously published sample analyses from Sinton et al. (2005), are available as a supplemental dataset.

2.3. ICP-MS analysis

Low-abundance trace elements were analyzed in selected samples by inductively-coupled, plasma mass spectrometry (ICP-MS) using the University of Hawai'i VG PlasmaQuad instrument. Clean rock chips were crushed in alumina, from which 0.1200 g were digested in a mixture of HNO_3, HCl and HF in sealed teflon CEM digestion vessels, using a microwave digestion oven at 90 psi. After digestion, the vessels were uncapped and heated to evaporate the solutions to near dryness, which were then diluted to ~100 g with 2% ultra-clean, distilled HNO_3. The solutions were stored in acid-cleaned plastic bottles until analyzed. Prior to analysis, samples were diluted 1:10 in 2% HNO_3. A mixed internal standard solution of Zn 67, In 115, and Bi 209, diluted to 1.0, 2.5, 5.0, and 10.0 ppb, in 2% HNO_3 was run along with each sample for instrument calibration. Samples were calibrated against international rock standards JB-3, NIM-N, JB-2, JGb-1 (Tables 2 and 3).

2.4. Mineral analyses by electron microprobe

Mineral compositions were determined using the University of Hawai'i Cameca SX-50 five-spectrometer electron microprobe, using an accelerating voltage of 15 kV, 20 nA beam current, and 10 μm beam

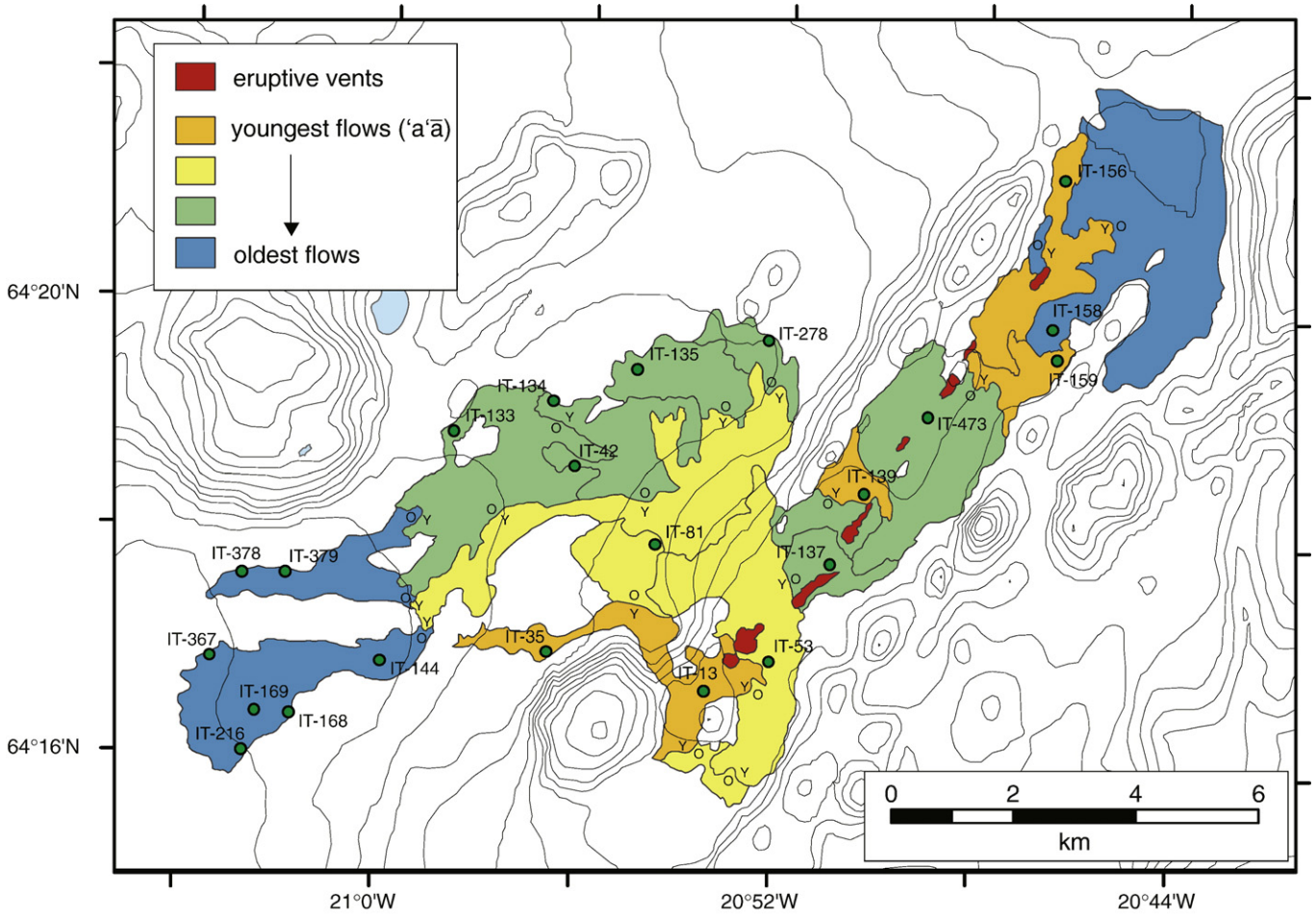

Fig. 3. Geologic map of Thjófahraun. Subunits defined on field relations (overlapping flows) and mineralogical differences. Y in Y–O pairings designates younger flows. Circles denote locations of samples with whole-rock XRF analyses. Topographic contours are in 20 m intervals.

diameter. Olivine and plagioclase analyses reported here are averages of a minimum of three spots collected from individual crystals (Table 4). Zoning profiles also were collected for selected plagioclase phenocrysts. A PAP-ZAF matrix correction was applied to all analyses.

Olivine was analyzed for Si, Mg, Fe, Ca, Mn and Ni using peak counting times of 60 s for Mg, Si, Ca and Fe, and 30 s for Mn and Ni. Background counting times were 30 s for Mg, Si, Ca and Fe, and 15 s for Mn and Ni. Samples were calibrated against San Carlos olivine (Mg), Springwater olivine (Fe), Verma garnet (Mn), diopside (Si and Ca) and Ni-metal (Ni) standards.

Plagioclase was analyzed for Si, Al, Fe, Mg, Ca, Na and K with peak counting times of 30 s for Si, Mg, Al and Na and 60 s for Fe, Ca and K. Background counting times were 30 s for Fe, Ca and K, and 15 s for Si, Mg, Na and Al. Na was analyzed first in each acquisition to minimize loss due to volatilization. Samples were calibrated against mineral standards Lake County plagioclase (Si and Al), San Carlos olivine (Fe and Mg), Amelia albite (Na), anorthite (Ca) and orthoclase (K).

2.5. Petrographic study

Thin sections were examined for textural indications of disequilibrium and 1000-point counts were collected on selected samples to determine mineral modes. Mineral grains <0.05 mm in size appear to have crystallized post-eruption, and are considered "groundmass" for counting purposes, so that our modes reflect the pre-eruptive phenocryst assemblage. Exceptions to this are some samples from Lambahraun whose groundmass has crystallized to sub-ophitic textures — modes from these samples represent an assemblage that has cooled relatively slowly after eruption. Modal data are reported in Table 5 with estimated errors ranging from <1 to 3% (Howarth, 1998).

3. Results and observations

3.1. Eruptive units and chronology

3.1.1. Thjófahraun

Thjófahraun lavas erupted from a highly effusive fissure system approximately 9 km long (Fig. 3). Radiometric carbon dating of charcoal remains beneath flows of this unit yields an age of 3680 ± 60 calibrated years B.P. (Sinton et al., 2005). About 1.0 km^3 of lava was erupted from 10 separate spatter cones aligned in a SW–NE trend. Lava channels up to 100-m wide are well developed close to eruptive vents, but we have not identified lava tubes or tube break-out structures in this unit.

We have divided the Thjófahraun field into 19 different subunits with boundaries defined by field observations and mineralogical differences (Fig. 3). All of the early phases of the eruption are pāhoehoe lava. Later units include some flows with transitional morphology. The youngest flow units are small-volume 'a'ā flows. Individual lava flows range up to 5 m thick, although many are less. Many of the subunits can be correlated to specific vent locations.

The relative age relations between subunits allow us to trace this eruption's chemical and mineralogical variability through time. Some of the oldest lavas make up the lower SW and NE-most portions of Thjófahraun. These subunits tend to be more olivine-phyric (up to 7%)

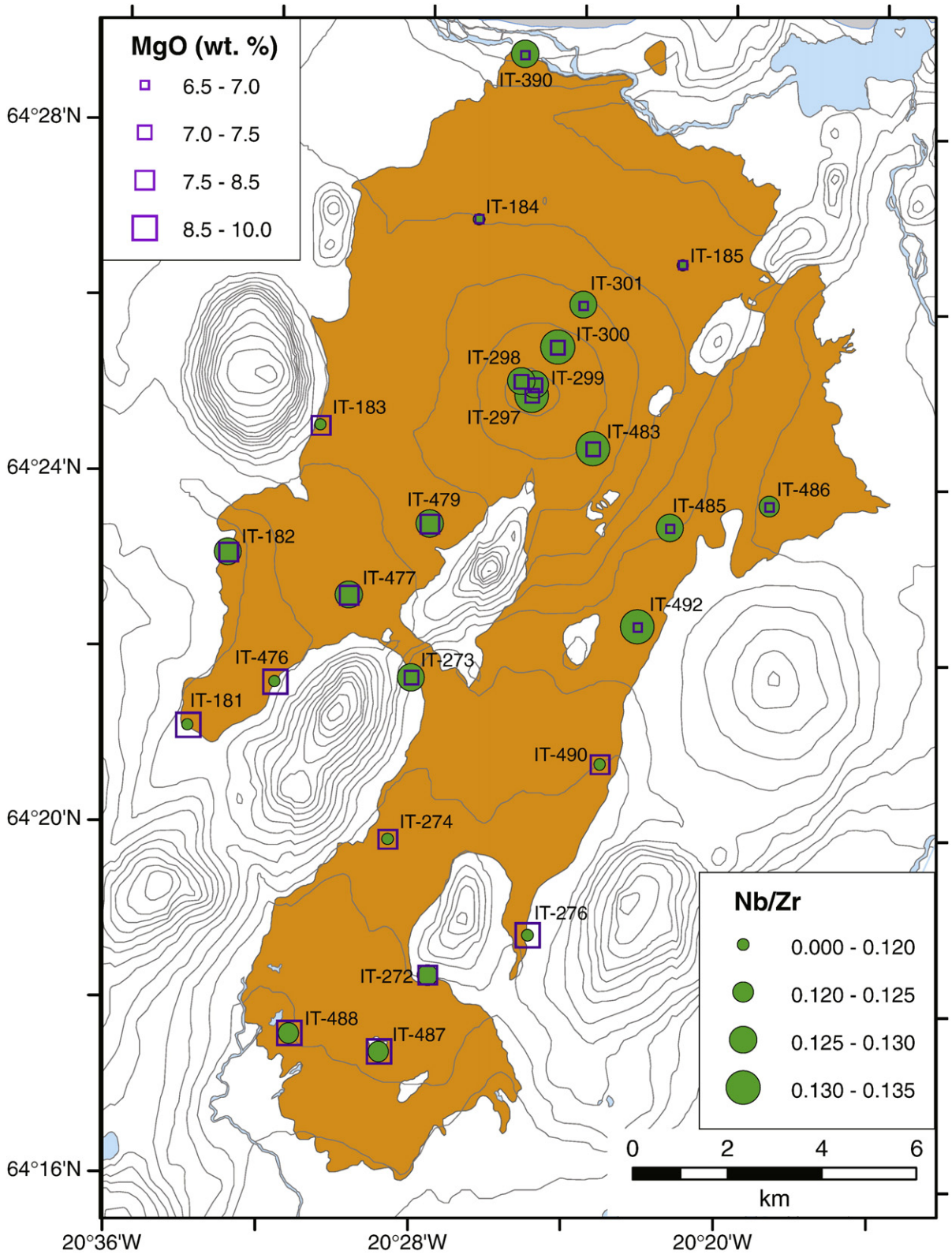

Fig. 4. Geologic map of Lambahraun. Sample locations with XRF analyses shown. Symbol size scales with Nb/Zr (circles) and MgO wt.% (squares). More distal samples tend to have higher MgO and lower Nb/Zr than samples closer to the vent. Topographic contours are in 20 m intervals.

and have slightly higher MgO contents than lavas in the SE. We are unable to determine age relations between the older NE and SW subunits, so it is difficult to say if there is an age sequence to vent activity, but both areas are generally older than the SE lavas based on stratigraphic field relations. The last lavas erupted are plagioclase-phyric 'a'ā lavas erupted from at least three vents spanning almost the entire length of the eruptive fissure system. These later lavas contain very little olivine (<3%), but more abundant plagioclase phenocrysts (5–7%). By comparison with the well-documented 1975–1984 fissure-fed Krafla Fires eruptive episode (Björnsson, 1985; Sæmundsson, 1991),

Table 1
Whole-rock XRF analyses.

Unit	Lambahraun											Thjófahraun				
Sample no.	IT-390	IT-476	IT-477	IT-479	IT-483	IT-485	IT-486	IT-487	IT-488	IT-490	IT-492	IT-13	IT-53	IT-137	IT-278	IT-473
Easting	0527548	0522666	0524173	0525844	0529247	0530936	0533027	0525108	0523195	0529601	0530315	0505300	0506340	0507290	0506190	0508819
Northing	7150977	7137528	7139409	7140971	7142661	7141047	7141556	7129769	7130099	7135985	7138932	7128150	7128665	7130275	7133885	7132715
SiO_2	48.80	47.40	48.15	48.18	48.54	49.03	48.78	48.17	47.60	47.99	48.88	48.41	48.41	49.26	48.51	49.03
TiO_2	2.13	1.85	1.86	1.61	1.75	1.86	1.62	1.88	1.89	1.66	2.28	1.87	1.73	1.91	1.77	1.78
Al_2O_3	13.98	15.14	14.97	16.41	15.99	15.91	17.06	15.14	15.05	15.70	13.84	14.94	15.46	15.47	15.07	15.46
FeO*	13.08	12.37	12.28	11.12	11.57	11.74	10.63	12.31	12.43	11.71	13.52	12.26	11.73	11.82	12.05	12.15
MnO	0.20	0.20	0.20	0.18	0.19	0.20	0.18	0.20	0.20	0.20	0.22	0.20	0.19	0.19	0.19	0.18
MgO	6.86	9.68	7.79	7.70	7.04	6.76	6.72	8.58	8.56	8.29	6.62	8.00	8.46	7.34	8.33	8.39
CaO	12.64	11.53	12.41	12.62	12.80	12.95	13.27	12.00	11.95	12.33	12.51	11.94	11.96	11.99	11.92	11.49
Na_2O	2.06	1.89	1.96	1.88	1.82	1.99	1.86	1.90	1.89	1.73	2.08	1.99	2.09	2.19	2.06	1.48
K_2O	0.21	0.16	0.18	0.17	0.17	0.18	0.16	0.17	0.17	0.13	0.21	0.23	0.21	0.24	0.23	0.18
P_2O_5	0.26	0.19	0.22	0.20	0.21	0.22	0.20	0.18	0.19	0.16	0.27	0.23	0.17	0.21	0.21	0.21
Sum	100.24	100.41	100.01	100.08	100.09	100.85	100.50	100.55	99.95	99.91	100.44	100.08	100.42	100.63	100.33	100.36
Sc	50	41	42	38	39	41	39	43	39	43	48	40	42	43	41	39
V	404	323	351	296	326	343	309	330	334	351	391	352	336	378	350	336
Cr	309	386	330	331	308	322	380	297	306	315	282	352	404	336	389	365
Co	46	55	50	45	43	42	41	47	47	50	46	46	51	45	51	49
Ni	64	176	108	114	90	76	84	121	124	129	64	122	157	107	140	160
Cu	–	102	–	–	–	–	–	109	106	–	–	–	–	–	–	–
Zn	108	104	102	83	91	93	83	99	98	101	109	98	100	102	102	99
Rb	3.8	3.3	3.3	3.1	3.3	3.1	2.9	3.3	3.2	3.3	3.5	4.6	3.9	4.8	4.4	4.0
Sr	195	198	193	208	204	203	208	189	191	187	202	190	185	203	193	200
Y	31	24	27	23	25	26	23	27	27	26	33	28	25	28	27	25
Zr	119	84	99	91	96	101	86	91	92	91	120	106	92	115	103	107
Nb	15.0	10.0	12.9	11.7	12.7	12.8	10.8	11.2	11.2	10.8	15.7	12.5	10.1	13.5	12.3	12.3
Ba	38	36	33	41	37	42	32	35	46	30	50	50	42	53	38	45

Oxide abundances in wt.%, trace elements in ppm. FeO* = total Fe expressed as FeO. Sample locations are given in WGS84 UTM coordinates.

Table 2
ICP-MS standards data.

n	JGb-1			JB-3			JB-2			NIM-N			B-THO		BIR-1
	6	*s*	Value	*3*	σ	Value	*3*	σ	Value	*4*	σ	Value	*3*	σ	Value
Ba	61	2.19	63	223	12.08	245	208	9.26	208	78.6	2.56	84	6.2	0.31	7.14
La	3.50	0.09	3.6	8.48	0.17	8.85	2.34	0.06	2.36	2.81	0.04	3	0.68	0.01	0.62
Ce	8.48	0.27	8	21.16	0.42	21.5	6.62	0.13	6.77	5.81	0.04	5.8	1.90	0.09	1.92
Pr	1.20	0.05	1.14	3.38	0.17	3.39	1.21	0.04	0.99	0.77	0.04	0.71	0.38	0.01	0.37
Nd	5.27	0.19	5.56	15.41	0.39	15.4	6.20	0.05	6.65	3.17	0.10	3	2.30	0.12	2.38
Sm	1.44	0.08	1.49	4.15	0.05	4.27	2.24	0.01	2.25	0.82	0.03	0.8	1.04	0.05	1.12
Eu	0.66	0.03	0.63	1.37	0.03	1.31	0.86	0.01	0.86	0.61	0.02	0.63	0.53	0.03	0.53
Gd	1.66	0.06	1.63	4.71	0.23	4.57	3.31	0.10	3.28	1.00	0.05	0.97	1.73	0.07	1.87
Tb	0.27	0.02	0.3	0.75	0.04	0.74	0.58	0.01	0.62	0.16	0.01	0.16	0.33	0.01	0.36
Dy	1.74	0.07	1.55	4.60	0.22	4.55	4.01	0.11	3.7	1.05	0.05	1.04	2.41	0.09	2.51
Ho	0.36	0.02	0.33	0.94	0.05	0.8	0.88	0.04	0.81	0.22	0.02	0.2	0.53	0.01	0.56
Er	0.99	0.05	1.06	2.63	0.14	2.61	2.57	0.11	2.62	0.64	0.03	0.66	1.56	0.05	1.66
Tm	0.14	0.01	0.15	0.38	0.03	0.41	0.37	0.01	0.43	0.09	0.00	0.1	0.23	0.01	0.25
Yb	0.92	0.04	1.02	2.45	0.09	2.62	2.52	0.10	2.51	0.63	0.02	0.67	1.54	0.06	1.65
Lu	0.14	0.01	0.15	0.37	0.03	0.39	0.39	0.02	0.39	0.10	0.01	0.1	0.23	0.01	0.25

Standard analyses given with number of runs (n) and standard deviation (σ). B-THO is a re-collected sample from the same locality as BIR-1. Accepted values are those of Govindaraju (1994).

Table 3
ICP-MS analyses.

Unit	Thjófahraun						Lambahraun			
Sample no.	IT-35	IT-35	IT-35	IT-133	IT-144a	IT-144a	IT-181	IT-182	IT-184	IT-184
Ba	56.6	58.1	59.2	53.5	58.8	57.7	40.7	49.2	46.4	48.9
La	8.42	8.65	8.76	8.04	9.53	9.38	6.26	8.54	7.83	8.31
Ce	21.1	22.0	22.2	19.9	23.2	22.8	15.9	21.0	19.5	20.6
Pr	3.03	3.12	3.18	2.86	3.44	3.39	2.48	3.20	2.96	3.12
Nd	13.6	14.1	14.2	12.9	15.0	14.6	11.3	14.1	13.1	13.8
Sm	3.76	3.88	3.91	3.51	4.20	4.17	3.29	3.99	3.72	3.90
Eu	1.41	1.46	1.50	1.33	1.59	1.53	1.33	1.53	1.44	1.51
Gd	4.27	4.35	4.45	4.16	4.92	4.75	3.97	4.61	4.42	4.60
Tb	0.71	0.75	0.76	0.69	0.85	0.83	0.69	0.80	0.76	0.80
Gd	4.41	4.55	4.63	4.27	5.05	4.91	4.07	4.73	4.51	4.70
Dy	4.58	4.72	4.81	4.40	5.19	5.05	4.22	4.86	4.70	4.93
Ho	0.95	0.97	0.98	0.90	1.09	1.07	0.88	1.01	0.98	1.04
Er	2.62	2.71	2.74	2.52	3.03	2.93	2.44	2.83	2.74	2.92
Tm	0.37	0.37	0.39	0.35	0.44	0.43	0.36	0.41	0.40	0.42
Yb	2.46	2.53	2.57	2.34	2.73	2.68	2.22	2.55	2.52	2.64
Lu	0.36	0.38	0.38	0.35	0.42	0.42	0.34	0.40	0.38	0.41

Table 4
Representative mineral analyses.

Representative analyses of plagioclase								
Unit	Lambahraun						Thjófahraun	
Sample anal.	IT-184[e]	IT-273[e]	IT-297			IT-300	IT-35	IT-133
			1	2	3			
SiO_2	45.7	47.5	48.8	47.3	47.4	49.7	48.6	49.0
Al_2O_3	34.0	32.8	31.8	33.0	32.7	31.2	32.1	31.7
FeO[a]	0.57	0.49	0.58	0.59	0.55	0.66	0.64	0.69
MgO	0.15	0.19	0.19	0.19	0.18	0.21	0.19	0.18
CaO	17.3	15.9	15.2	16.3	16.0	14.3	15.3	15.2
Na_2O	1.47	2.18	2.73	2.09	2.37	3.15	2.60	2.76
Total[b]	99.2	99.0	99.3	99.5	99.2	99.2	99.4	99.5
Cations on the basis of 8 oxygens								
Si	2.127	2.202	2.253	2.188	2.198	2.292	2.242	2.260
Al	1.865	1.792	1.730	1.799	1.787	1.696	1.746	1.723
Fe	0.010	0.009	0.010	0.010	0.010	0.011	0.011	0.012
Mg	0.010	0.013	0.013	0.013	0.012	0.014	0.013	0.012
Ca	0.863	0.789	0.754	0.808	0.795	0.706	0.756	0.749
Na	0.133	0.196	0.244	0.187	0.213	0.282	0.233	0.247
Total	5.007	5.000	5.004	5.006	5.015	5.001	5.001	5.002
AnM[c]	86.7	80.0	75.4	81.1	78.7	71.3	76.4	75.0

Representative analyses of olivine								
Unit	Lambahraun						Thjófahraun	
Sample anal.	IT-182	IT-273[e]		IT-276	IT-297	IT-300	IT-35	IT-133
		1	2					
SiO_2	38.9	38.4	38.2	37.7	38.6	38.3	39.4	38.9
FeO[a]	17.3	19.2	19.5	21.9	19.9	21.3	17.0	16.3
MnO	0.26	0.31	0.29	0.32	0.27	0.31	0.25	0.36
MgO	43.5	41.5	41.5	39.4	40.7	39.8	43.0	44.0
CaO	0.29	0.36	0.33	0.35	0.34	0.39	0.29	0.28
NiO	0.16	0.14	0.12	0.10	0.10	0.07	0.14	0.22
Total	100.4	99.9	99.9	99.8	99.9	100.2	100.1	100.1
Cations on the basis of 4 oxygens								
Si	1.039	1.047	1.044	1.054	1.057	1.059	1.051	1.035
Fe	0.174	0.197	0.201	0.230	0.205	0.222	0.171	0.163
Mn	0.006	0.007	0.007	0.008	0.006	0.007	0.006	0.008
Mg	1.731	1.687	1.692	1.642	1.662	1.640	1.710	1.746
Ca	0.008	0.011	0.010	0.010	0.010	0.012	0.008	0.008
Ni	0.003	0.003	0.003	0.002	0.002	0.002	0.003	0.005
Total	2.961	2.953	2.956	2.946	2.943	2.941	2.949	2.965
Fo[d]	81.7	79.4	79.1	76.2	78.5	76.9	81.9	82.8

[a] Total Fe as FeO.
[b] K_2O for all plagioclase analyses is below detection limit = 0.017 wt.%.
[c] An = Ca*100/(Ca + Na + K).
[d] Fo = Mg*100/(Mg + Fe).
[e] Lambahraun sample with plagioclase accumulation.

the flow field was probably produced during a series of short-lived (days to weeks) eruptive events that together comprise a major rifting episode. Although the exact duration of this episode is not known, estimates of effusion rates for pāhoehoe and 'a'ā lavas (Rowland and Walker, 1990) indicate a total eruption time for the complete 1 km^3 of Thjófahraun lava on the order of months to years.

3.1.2. Lambahraun lava shield

Lambahraun is a moderately large, monogenetic, low-angle lava shield covering >140 km^2, with an estimated 7.3 km^3 of erupted lava (Fig. 4). Radiometric dating from two separate localities gives an average age of 4100 ± 500 years B.P. (Sinton et al., 2005). Lambahraun mainly consists of dense pāhoehoe lava in hundreds of thin flow units that likely formed at low effusion rates (Rowland and Walker, 1990; Rossi, 1996). The large erupted volume and inferred low average eruption rate suggests that this lava shield was produced over a period of several decades. Although the field mainly consists of on-lapping flow units, there are no mappable subunits within it. Furthermore, large hornito spires are common around the summit caldera and we have identified at least one major tube breakout elsewhere in the flow field. Thus, tube-fed lavas are probably more common in Lambahraun than in Thjófahraun and correlation of individual samples with time during eruption is more equivocal. Lambahraun lavas tend to be more porphyritic than Thjófahraun lavas with little indication for any systematic spatial correlation of its mineralogy. Many samples are nearly holocrystalline, particularly in the interiors of tumuli, indicating relatively slow cooling after eruption.

Although we are unable to define a strict eruption chronology for Lambahraun, the flow field is areally zoned with respect to several chemical parameters. Samples from the SW portions of the flow field tend to have higher MgO and lower Nb/Zr than those closer to the summit vent in the NE (Fig. 4). Despite the complications that tube-fed lava adds to determining an eruption chronology, in general the more distal SW lavas appear to have erupted earlier than the more evolved lavas N and E of the summit caldera. The spatial relationships therefore suggest that the erupted magma generally became progressively more differentiated with higher Nb/Zr during the course of the eruption. Late eruption of more differentiated magma has also been observed in other WVZ lava shields (Sinton et al., 2005) and elsewhere in Iceland (Moore and Calk, 1991).

Table 5
Petrographic modes. Rock modes based on 1000-point counts.

Unit	Relative phase abundance (%)						
	Sample	ol	plag	cpx	Groundmass	Vesicles	Total
Lambahraun	IT-181	5.9	8.5	0.2	70	15.4	100.0
	IT-182	0.2	7.6	–	74.4	17.8	100.0
	IT-183[a]	22.7	36.2	3.6	15.4	22.1	100.0
	IT-185	1.6	4.4	0.1	87	6.9	100.0
	IT-274[a]	12.6	20.6	5.5	43.5	17.8	100.0
	IT-298[a]	23.4	34.8	3.6	25.1	13.1	100.0
	IT-299	1.4	3.1	–	75.5	20	100.0
	IT-301	2.8	16.2	0.7	57.8	22.5	100.0
	IT-483[a]	6.4	19.1	1.5	54.5	18.5	100.0
	IT-485[a]	6	17.2	1.3	58	17.5	100.0
	IT-486[a]	7.7	14.8	–	53.2	24.3	100.0
	IT-487	3.8	3.8	–	69.2	23.2	100.0
	IT-490[a]	9.3	13.6	0.4	63.6	13.1	100.0
	IT-492[a]	18.7	29.3	5.6	26.3	20.1	100.0
Thjófahraun	IT-35	2.8	5.9	–	76.9	14.4	100.0
	IT-42A	1.8	1.1	–	79.8	17.3	100.0
	IT-42B	2.0	1.3	–	78.5	18.2	100.0
	IT-81	1.7	2.7	–	75.5	20.1	100.0
	IT-133	2.2	0.3	–	87.2	10.3	100.0
	IT-134A	1.3	0.4	–	82.2	16.1	100.0
	IT-135	2.9	1.2	–	79.5	16.4	100.0
	IT-139	1.3	4.1	–	79.3	15.3	100.0
	IT-144A	2.5	1.6	–	86.2	9.7	100.0
	IT-156	4.1	6.8	–	71.4	17.7	100.0
	IT-158	3.4	0.1	–	78.7	17.8	100.0
	IT-159	2.2	6.3	–	76	15.5	100.0
	IT-169	1.8	0.9	–	90.1	7.2	100.0
	IT-367	3.2	1.1	–	87.8	7.9	100.0

[a] Sample has coarse groundmass. Point counts not representative of phenocryst assemblage.

3.2. Chemical variations

3.2.1. Crystal fractionation

Olivines in both Thjófahraun and Lambahraun appear to be in equilibrium with their host rocks (Roeder and Emslie, 1970) based on mineral and whole rock compositions. Groundmass olivines and rims on olivine phenocrysts commonly have slightly lower forsterite (Fo = Mg*100/(Mg + Fe)) contents than phenocryst cores, consistent with later crystallization. Plagioclase phenocrysts tend to have normal or oscillatory zoning, and some of the larger phenocrysts have a sieved texture. Thjófahraun plagioclase grains have significantly lower An content for a given rock MgO or coexisting olivine Fo content than Lambahraun plagioclase. We interpret this to reflect the lower CaO of the melt from which they crystallize, as Thjófahraun lavas have lower CaO contents than Lambahraun at the same MgO (Fig. 5), while Na and Al contents are not significantly different.

The whole-rock chemical variation of Thjófahraun is broadly consistent with evolution by shallow crystal fractionation. Analyzed samples span a range of ~1.5 wt.% MgO around a median of 8.0 wt.%, and exhibit limited chemical variability at a given MgO (Fig. 5). While lava compositions are more restricted in MgO than for Lambahraun, the range of values at a given MgO appears to be greater. Although plagioclase occurs in some of the samples, CaO and Al_2O_3 values anti-correlate with MgO, suggesting that Thjófahraun magmas did not fractionate plagioclase prior to eruption. Early Thjófahraun flows have compositions spanning the entire spread of MgO. Late-stage 'a'ā lavas have relatively low MgO with limited chemical variability (Fig. 5). These results suggest early eruption from a relatively poorly mixed magma chamber, followed by later eruptions that tapped a more homogeneous and probably smaller volume of more differentiated magma.

The major and trace element variation of Thjófahraun whole rocks can be modeled by simple fractionation scenarios using MELTS (Ghiorso and Sack, 1995; Smith and Asimow, 2005). The best-fit model run contains 0.4 wt.% H_2O for a crystallization pressure of 1 kb (QFM-2). A value of 0.4 wt.% is within the range expected for Iceland magmas (e.g., Schilling et al., 1983; Metrich et al., 1991; Nichols et al., 2002), although MELTS runs with lower water contents are also able to approximate the observed trends at slightly higher pressures (1.5–2 kb). Note that there is some uncertainty in the water content due to the interplay with the model pressure, because both higher water content and higher pressures suppress the appearance of plagioclase on the liquid line of descent. Although we biased our analyses to the least phyric samples, the data reported are for whole rocks, and therefore not true liquid compositions.

Lambahraun samples show a greater variation in MgO than Thjófahraun (~2.5 wt.% MgO), and are significantly lower in K_2O, Rb, Y and Zr, and higher in CaO than Thjófahraun lavas for the same MgO. Overall chemical variations within Lambahraun are more complicated than for Thjófahraun. For example, there are two distinct populations of Lambahraun samples on Al_2O_3, FeO and TiO_2 vs. MgO (Fig. 5). Also, both CaO and Nb/Zr increase with decreasing MgO, despite widespread presence of plagioclase in Lambahraun lavas. Thus, several features of Lambahraun are inconsistent with simple low-pressure fractionation of the mineral phases observed in the lava, especially at low MgO.

3.2.2. Crystal accumulation in Lambahraun lavas

Some Lambahraun samples have higher Al_2O_3 and CaO and significantly lower FeO, TiO_2, P_2O_5, and to a lesser degree K_2O (open symbols, Fig. 5), than the main trend of most samples from this unit. These same samples also tend to be low in Mn, Sc, V, Zn, Y, Zr and Nb, while exhibiting slightly higher Sr. Such variation is not consistent with crystal fractionation, but can be explained by up to 15% accumulation of plagioclase in these whole-rock samples. The amount of plagioclase accumulation has been evaluated by linear subtraction of a representative plagioclase composition (IT-273 analysis in Table 4) from these sample compositions along a path of constant Mg# until the liquid intersects the main liquid line of descent. The amount of plagioclase subtracted ranges from 5 to 15%, and is in all cases less than the amount of modal plagioclase in the sample (Table 6, Fig. 6). The part of the system where excess plagioclase was accumulated is poorly constrained but presumably could occur by gravitative or dynamic processes in a magma reservoir, during transport to the surface, or in lava flows after eruption. The latter interpretation is supported by the observation of substantial variations in plagioclase abundance over scales of a few decimeters within individual tumuli of the flow field, although this observation does not preclude the possibility that some accumulation could be pre-eruptive.

Among the most surprising features of the Lambahraun data are steady increases in CaO, highly incompatible element abundances, and incompatible element ratios such as Nb/Zr with decreasing MgO (Fig. 7). Although some major element trends (e.g., Al_2O_3, FeO) indicate plagioclase fractionation has occurred, CaO abundances are higher than would be predicted by simple crystal fractionation alone, even after correcting for plagioclase accumulation. Low-pressure crystal fractionation paths predicted by MELTS (Ghiorso and Sack, 1995; Smith and Asimow, 2005) yield CaO and incompatible element values significantly lower than the observed trends (Fig. 7). While crystallization at slightly higher pressures can lead to higher CaO contents due to the delay in plagioclase crystallization, this is inconsistent with other major element trends, particularly that of Al_2O_3. CaO will become even more depleted at higher pressures of fractionation because of the early crystallization of Ca-rich pyroxene at high pressure. These results indicate that Lambahraun lava compositions are inconsistent with the combined effects of crystal fractionation and plagioclase accumulation.

The progressive increase in CaO and decrease in Al_2O_3 with decreasing MgO requires the addition of a Ca-rich, Al-poor component, such as clinopyroxene, in this process. Multiple linear regression of the major elements indicates a net addition of ~5% clinopyroxene for the total range of MgO concurrent with olivine and plagioclase removal to

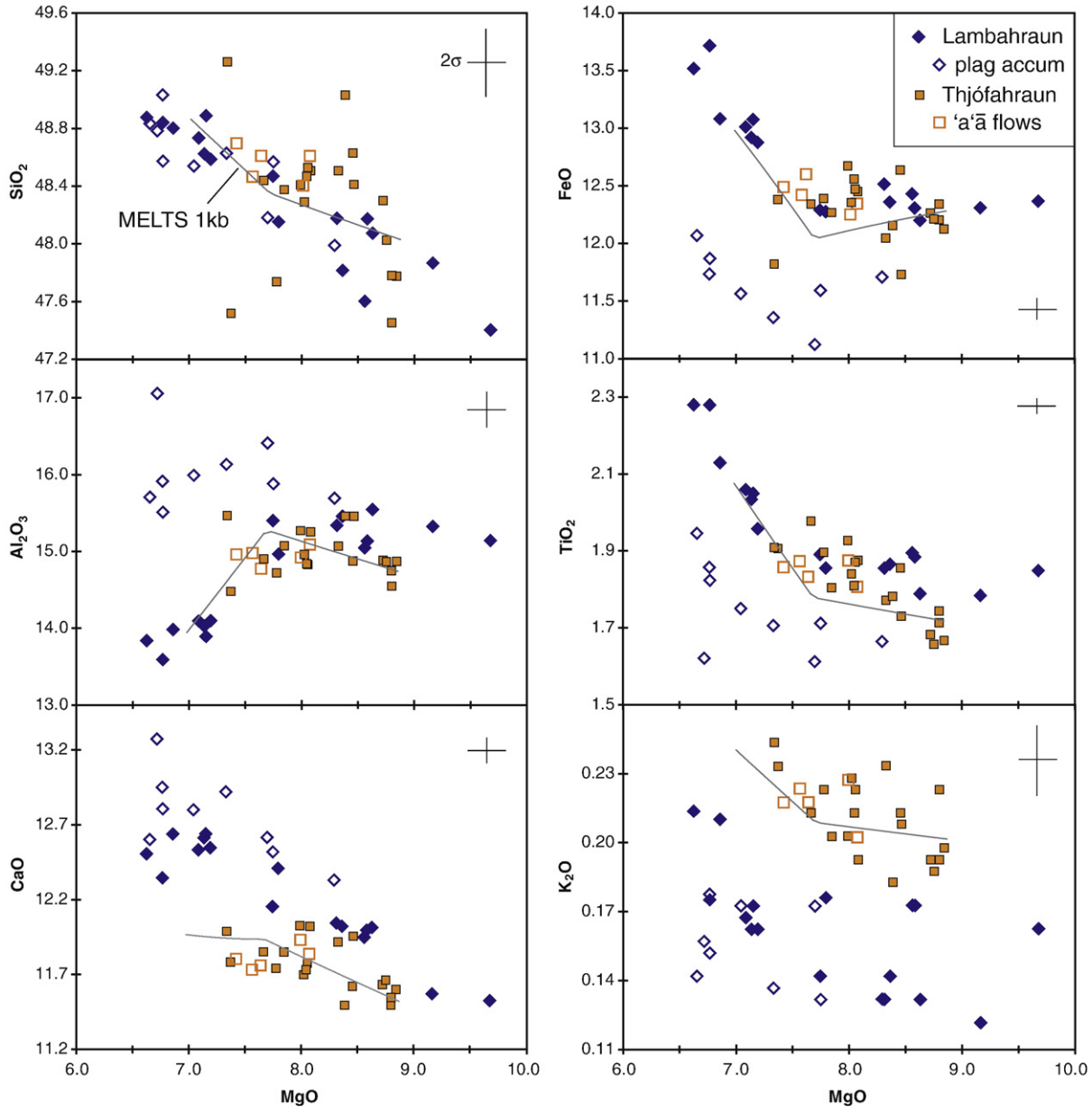

Fig. 5. Major element chemical variations of Thjófahraun (squares) and Lambahraun (diamonds). Open diamonds are Lambahraun samples displaced from the main trend, which we interpret to be affected by plagioclase accumulation (see text for discussion). Open squares denote Thjófahraun late-stage 'a'ā flows. Solid line shows 1 kb fractionation model for Thjófahraun determined by the Adiabat_1ph version of MELTS (Ghiorso and Sack, 1995; Smith and Asimow, 2005) with oxygen fugacity of QFM-2 and 0.4 wt.% H_2O in the starting magma (IT-133). Crosses in each panel denote 2σ uncertainty in analytical data.

explain the high CaO and other major element values in the more evolved rocks (Table 7). As crystal accumulation has already been shown to play a role in Lambahraun's evolution, and there is both petrographic and chemical evidence for clinopyroxene accumulation in selected other Icelandic lava flows (Maclennan, 2008a; Halldórsson et al., 2008a,b), it is appropriate to consider whether the progressive enrichment in CaO and incompatible elements can be accounted for by increasing amounts of clinopyroxene accumulation with decreasing MgO content, despite a lack of petrographic evidence for this process in Lambahraun samples. The thin dashed line in Fig. 7 shows a predicted evolutionary trend calculated by addition of increasing amounts of clinopyroxene, up to a total ~5% accumulation predicted from mass balance at low MgO, to the MELTS-predicted fractionation run. This predicted trend fits the major element data better than fractionation ± plagioclase accumulation alone, but only at MgO values greater than ~7.5 wt.% MgO, below which clinopyroxene accumulation and the MELTS-predicted clinopyroxene fractionation paths are co-linear. Although the major element data could be reconciled with clinopyroxene accumulation to magmas that failed to fractionate

Table 6
Plagioclase accumulation in Lambahraun samples (mass fractions).

Sample	Modal plag	Modeled accum
IT-183	0.43	0.06
IT-273	0.20	0.08
IT-184	0.15	0.07
IT-301	0.20	0.08
IT-479	0.19	0.10
IT-483	0.22	0.09
IT-485	0.19	0.09
IT-486	0.18	0.15
IT-490	0.14	0.05

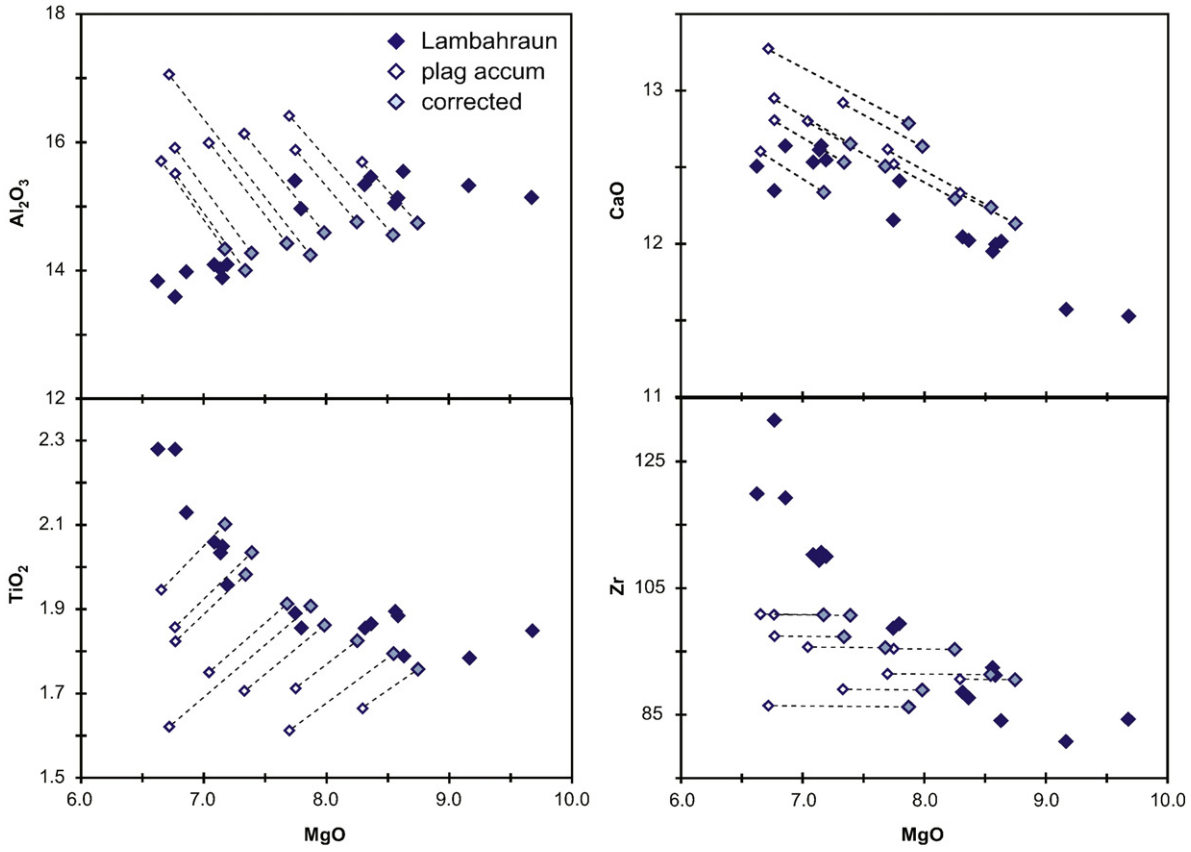

Fig. 6. Correction for plagioclase accumulation in Lambahraun samples. Sample compositions corrected back to the main liquid line of descent for Lambahraun (solid symbols) along lines of constant Mg# using an average plagioclase composition. Open diamonds are uncorrected values, shaded diamonds are corrected compositions.

clinopyroxene, e.g., magmas that crystallized clinopyroxene crystals that were not fractionated, this process produces striking misfits to the trace element variations. Incompatible elements such as Nb and Zr show under-enrichments at lower MgO, and trace elements that are less incompatible in clinopyroxene, like V and Sc, exhibit striking over-enrichments.

Taken together, there is both petrographic and chemical evidence for accumulation of excess plagioclase crystals in some Lambahraun rocks, and visual evidence in outcrops that plagioclase crystals are mobile in surface lava flows of this unit. Although clinopyroxene accumulation produces slightly better fits to major element data, it produces greater misfits in trace element variations. Thus, although clinopyroxene accumulation has been well documented in some Icelandic lava flows, we lack both petrographic and chemical evidence that it has been important in controlling the unusual Lambahraun chemical variation.

3.2.3. Evidence for partial melting processes in Lambahraun chemical evolution

In addition to the enrichment in CaO and Nb at low MgO values, are enrichments in light rare earth elements (REE) (Fig. 8). The magnitude of enrichment for a given element is approximately inversely correlated with melting partition coefficients for these elements, such that the most highly incompatible elements Nb, Zr, La, Ce show the greatest enrichment at low MgO. We calculate the effective over-enrichment for elements *i* in a low-MgO Lambahraun composition (6.7 wt.%) as $\varepsilon_i = C_i/C_i^*$, where C_i is the concentration of element *i* in the sample, and C_i^* is the expected concentration of that element from crystal fractionation. There is a clear negative correlation between the cpx-liquid partition coefficient ($K_d^{cpx\text{-}liq}$) and the degree of over-enrichment (ε_i) (Fig. 9). The relationship between trace element incompatibility and the relative misfits of Lambahraun data from predicted crystal fractionation trends is consistent with partial melting, and opposite of what one would expect for clinopyroxene crystal accumulation in the proportion required by the major element linear regression analysis (Fig. 9). We therefore consider various scenarios in which a partial melting process may contribute to Lambahraun's geochemical evolution. This partial melting signature could be produced either in mantle melting, e.g., by variable melting or source variations, or by reaction in the crust. In this section, we outline and evaluate different mechanisms by which apparent coupling between magma evolution and enrichment via partial melting could occur.

Simple magma mixing between incompatible element-depleted, high-MgO magma and incompatible element-enriched, low MgO magma should produce linear chemical variation vs. MgO, as seen, for example, in the variation trends of P and Nb. However, many element trends exhibit distinct kinks correlated to fractionating phases or curved relations with MgO (e.g., Al_2O_3, TiO_2, FeO, Sc, V). Additionally, spatial variations in the Lambahraun flow field (Fig. 4) suggest that low-MgO lavas with the highest Nb/Zr ratios were erupted late in the sequence of the volcano. Thus, the inferred eruptive sequence and chemical variations are inconsistent with progressive recharge where the most recent magma would be expected to be more Mg-rich than the resident magma.

A slightly different scenario is that incompatible element-depleted resident magma is progressively diluted with more enriched recharge magma prior to or concurrent with crystal fractionation. Concurrent mixing and crystallization was proposed by Maclennan (2008a) to explain olivine melt inclusion data from the Northern Volcanic Zone in Iceland. However, although the relative trace element enrichments are correlated with $K_d^{cpx\text{-}liq}$, they also are associated with enrichment of CaO, which would not be expected from variable partial melting of

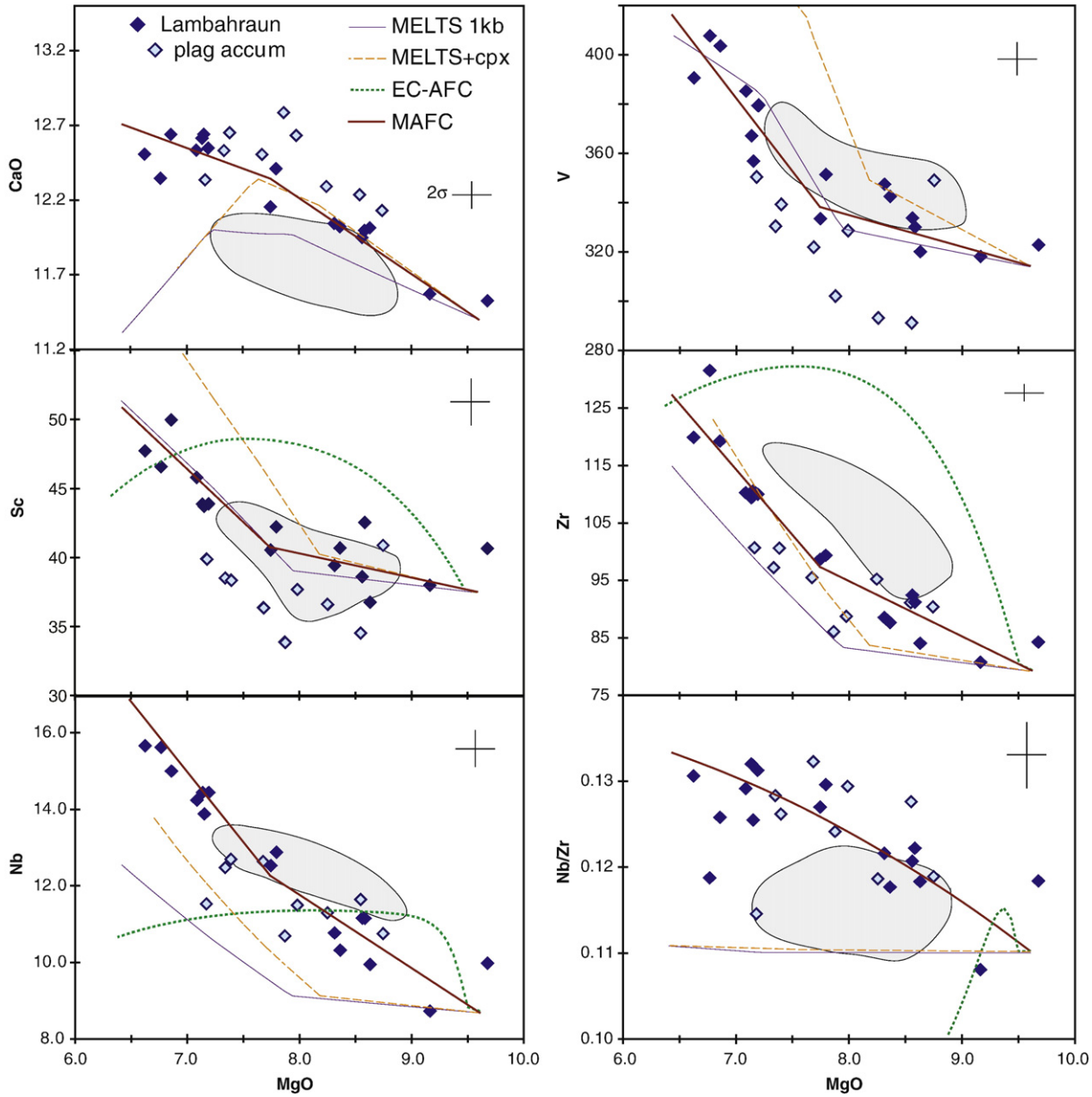

Fig. 7. Selected chemical variations of Lambahraun; shaded diamonds are sample compositions that have been corrected for plagioclase accumulation (see text and Fig. 6). Thjófahraun data shown as gray fields. Thin solid line is the MELTS fractionation model for Lambahraun (see Fig. 5 caption for run conditions); thin dashed line is the MELTS fractionation trend plus the addition of increasing amounts of clinopyroxene accumulation (see text for discussion); dotted line shows energy-constrained AFC model using equations of Spera and Bohrson (2001); thick solid line is the MAFC model calculation which simulates crustal interaction during melt migration by "refreshing" wallrock composition in each step (see text for description of calculation). Wallrock composition and other details of the AFC and MAFC models are given in Table 8.

Table 7
Linear regression of Lambahraun evolution.

	Parent	Daughter	ol	plag	cpx	Predicted melt comp.
	IT-181	IT-185				
SiO_2	47.87	48.84	40.14	46.73	53.58	48.83
TiO_2	1.78	2.28	0	0	1.12	2.22
Al_2O_3	15.33	13.59	0	34.16	4.01	13.59
FeO	12.31	13.72	11.46	0.40	6.37	13.74
MnO	0.19	0.22	0.24	0	0.10	0.25
MgO	9.16	6.77	47.00	0	15.45	6.77
CaO	11.57	12.35	0.30	17.10	20.03	12.37
K_2O	0.12	0.18	0	0.02	0	0.19
P_2O_5	0.16	0.26	0	0	0	0.24
	Predicted contributions		−0.11	−0.14	0.05	

Negative predicted contributions represent net fractional crystallization of the mineral phase; positive values represent net addition (assimilation).

a common upper mantle assemblage. Therefore, if Lambahraun variations reflect mixing of melts derived from mantle melting, the source mantle must be heterogeneous on a very small scale and produce differing primary magma compositions over a timescale of decades. Although there is evidence for heterogeneities in the mantle under Iceland (Zindler et al., 1979; Hémond et al., 1993; Stracke et al., 2003; Thirlwall et al., 2004; Maclennan, 2008a), preliminary isotopic data (Halldórsson et al., 2008b) indicates that the source mantle for Thjófahraun and both high-Nb/Zr and low-Nb/Zr Lambahraun lavas are isotopically similar. Thus, if mantle heterogeneity is responsible for varying incompatible element ratios in Lambahraun, the trace element heterogeneity must be decoupled from isotopic ratios, and progressive recharge must be accompanied by an increase in fractionation.

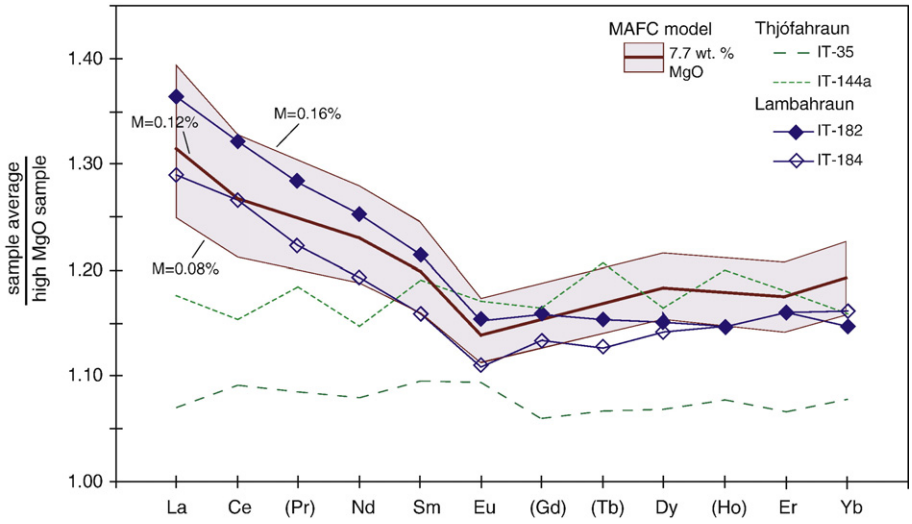

Fig. 8. Selected rare earth elements (REE) for Lambahraun and Thjófahraun samples normalized to the highest MgO sample analyzed by ICP-MS for their respective units (IT-181 for Lambahraun, IT-133 for Thjófahraun). Elements in parentheses not included in modeling. Relatively flat patterns for Thjófahraun samples with total REE abundance increasing with decreasing MgO are consistent with fractionation. Note the pronounced enrichment in light REE relative to heavy REE in Lambahraun samples with low MgO. Model runs represent mixing of 0.1% partial melting of wallrock in each increment of −0.1 wt.% MgO, shown for a range of mixing proportions (M = ratio of anatectic to primary melt).

3.3. Crustal interaction in Lambahraun magmas

An alternative process that couples incompatible element enrichment and decreasing Mg# is melt–wallrock interaction during melt migration and/or storage in the crust. Our major element mass balance results indicate combined addition of a clinopyroxene component coupled to fractional crystallization of plagioclase and olivine. Because the magnitudes of enrichment are approximately inversely correlated with clinopyroxene-liquid partition coefficients (Fig. 9), the clinopyroxene assimilant must be in the form of clinopyroxene-dominated melts, rather than whole-scale digestion of clinopyroxene crystals. In this regard, the process is similar to concurrent assimilation and fractional crystallization (AFC) (e.g. DePaolo, 1981; O'Hara, 1995, 1998; Spera and Bohrson, 2001).

Most AFC models assume constant pressure, such as a resident magma chamber that reacts with surrounding wallrock. The composition of the anatectic (wallrock-derived) melts follow melting functions based on the partition coefficients of each element, so that the earliest

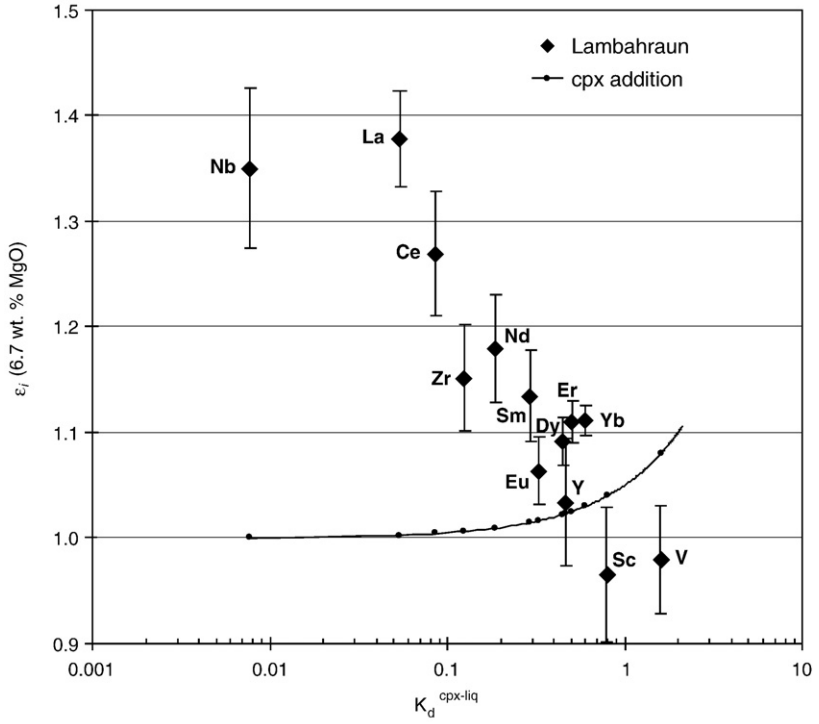

Fig. 9. Plot of enrichment factors (ε_i) for selected trace elements at 6.7 wt.% MgO vs. clinopyroxene-liquid partition coefficient ($K_d^{cpx\text{-}liq}$). Enrichment factor for each element calculated as $\varepsilon_i = C_i/C_i^*$, where C_i is the concentration of element i in the sample, and C_i^* is the expected concentration of that element from crystal fractionation; error bars denote root mean square deviation of ε_i–MgO for all samples. Black line shows values for accumulation of 5% clinopyroxene crystals. The result indicates that Lambahraun incompatible element enrichment is consistent with partial melting of clinopyroxene, and not accumulation or digestion of clinopyroxene crystals.

anatectic melts are the most enriched in incompatible elements, followed by a gradual decline in incompatible element concentration as they are stripped from the surrounding wallrock. This process results in concave down incompatible element vs. MgO variation curves for the magma (Fig. 7) that differ from observed Lambahraun sample data, which show a steady, continuous increase in incompatible element concentrations with MgO-variation trends that are linear to concave up.

To avoid the inevitable depletion in incompatible elements that occurs during reaction with a static wallrock, we envision a process that allows the crustal assimilant to remain relatively undepleted by prior melting. In a magma chamber setting, this might occur if partially melted wallrock is progressively stoped into the convecting interior of the chamber, exposing new wallrock for partial melting. However, we see no physical evidence for partially digested wallrock, and complete digestion should have strong effects on the major element chemical variability, depending on the mode of the digested crustal material. While we have not fully explored the chemical consequences of this process, we propose instead that wallrock melting occurs during melt migration through the crust, which eliminates the need to account for undigested crustal material. In this model, partial melts of wallrock are assimilated over a range of pressures determined by the initial temperature and solidus of the wallrock, and the amount of heat conducted from a migrating melt into its surroundings. This process naturally increases the melt's incompatible element concentration by continually introducing fresh, unmelted wallrock to the anatexis process as the surrounding crust heats above its solidus. Hereafter, we refer to this process as migrating AFC (MAFC).

3.4. Assimilation modeling

To model the MAFC process, we utilize equations of nonmodal fractional melting and crystallization (Shaw, 1970) in a simple, stepwise calculation. By discretizing the problem into small steps in melt MgO content (equivalent to small steps of temperature of the cooling melt), we can model crystallization of the magma and mix in variable proportions of melted wallrock, tracking the combined effects on melt composition. Crystallizing phase proportions are determined from the major element compositional variations. We define two crystallization regimes (olivine only and olivine + plagioclase) based on a distinct kink in MgO variation trends when plagioclase joins the crystallizing assemblage (~7.76 wt.% MgO). Average crystallizing proportions of olivine (MgO > 7.76) or olivine + plagioclase (MgO < 7.76) from linear regressions of these two separate portions of the major oxide trends can be divided into crystal fractions per unit MgO. For each small step in MgO, we calculate the change in incompatible element composition of the melt from fractional crystallization of the relevant phases (olivine ± plagioclase) and mix in a small proportion of melt derived from nonmodal fractional melting of wallrock. Olivine, plagioclase and clinopyroxene proportions in the wallrock (X's in Table 8) are set to the CIPW norm of average WVZ basalt from Sinton et al. (2005). We derived the wallrock trace element composition using the dynamic melting model for the Iceland WVZ of Sinton et al. (2005), with ~2% melting in the garnet field followed by 10% melting in the spinel field of primitive mantle (Sun and McDonough, 1989). Lacking further constraints on the crustal composition beneath Lambahraun, we choose this composition as representing an average crustal composition under the WVZ. This is a simplification of what is certain to be a heterogeneous crust whose composition changes with depth, quite possibly in nonsystematic ways. To simulate the effects of melt migration, we "refresh" the wallrock, so that the initial composition for each AFC step is the original, unmelted crustal composition. Using the melt–solid partition coefficients given in Table 8, we calculate the compositional evolution of selected trace elements (Sc, V, Y, Zr, Nb, La, Ce, Sm, Eu, Dy, Yb and Lu) assuming the melting mode (p's in Table 8) is dominated by clinopyroxene. Results are plotted in Figs. 7 and 8.

Table 8
MAFC model partition coefficients and melting parameters.

Partition coefficients				Starting compositions	
Mineral	ol	plag	cpx	C_0	C_{wr}
Sc	0.33	0.025	0.8	38	30
V	0.3	0.01	1.6	318	300
Y	0.023	0.027	0.467	23	28
Zr	0.004	0.0128	0.1234	80	83
Nb	0.001	0.04725	0.0077	8.8	4
				(IT-181)	
La	0.000007	0.08	0.0536	6.26	4
Ce	0.00001	0.1	0.0858	15.9	12
Nd	0.00007	0.1	0.1873	11.3	11
Sm	0.0007	0.0845	0.291	3.29	2.8
Eu	0.00095	0.2	0.33	1.33	1.1
Dy	0.004	0.06	0.45	4.22	4
Er	0.009	0.02	0.50	2.44	1.9
Yb	0.02	0.02	0.60	2.22	2.5
Melting parameters					
X_{wr} (%)	7.8	57.7	34.4		
p (%)	5	5	90		

Proportions of crystallizing phases taken from major element linear regression. Partition coefficients from compilation of Keleman et al. (2003), Dunn and Sen (1994), Green (1994), Jones (1995), McKenzie and O'Nions (1991, 1995). Crustal mode (X_{wr}) determined from the CIPW norm calculation of average WVZ basalt (Sinton et al., 2005).

Due to the trade-off between extent of anatectic melting (F_m) and the mixing proportion (M = ratio of anatectic melt to primary magma), there is a range of conditions over which the model can approximate the observed data. Best-fit model runs have relatively low mixing proportions (M ~ 0.08–0.16% of partial melt added in each step) and a fairly broad range of permissible F_m values (<0.1–5% partial melting of wallrock at each step), resulting in a total contribution of 3–5% anatectic melt over the observed range of sample MgO (9.6–6.6 wt.% MgO). We assume melting to be dominated by clinopyroxene, as required by the ~5% addition of clinopyroxene indicated by major element linear regression. Although the values we used (p's in Table 8) are somewhat arbitrary, the model is relatively insensitive to the melting mode, and a wide range of mineral contributions to the melt can produce the observed chemistry. Results for some of the more incompatible elements can be strongly affected by accessory minerals present in the wallrock, as their presence can greatly affect bulk D's for certain elements. The model we present in Figs. 7 and 8 contains olivine, plagioclase and clinopyroxene proportions as determined above. At such low degrees of partial melting, the model is far more sensitive to the chosen partition coefficients than the X's so, although we have assumed a single wallrock composition for this exercise, a wide range of bulk crustal compositions could give similar results. Olivine can range from 5 to 30%, plagioclase from 30 to 65%, and clinopyroxene from 25 to 60%, and still reasonably approximate the observed data within the uncertainties of the model. Because the model predictions are so sensitive to partition coefficient values (particularly for the more incompatible elements) and these are not all well-known, this is our greatest source of uncertainty.

It is important to note that our MAFC model is not thermodynamically constrained, nor does it take into account the amount of heat actually available for melting or the chemical potentials of the phases involved. Coupling thermodynamic constraints with the geochemical evolution of the individual phases, i.e., incorporating heat conduction from the migrating melt into its surroundings, the latent heat of crystallization, and pressure-dependent phase equilibria, are worth investigating, although beyond the scope of this paper. The simplified model presented here shows that the observed geochemical trends can be reproduced with reasonable extents of melting and fractionation and a suitable wallrock composition, recognizing that the magnitude of the geochemical effects of this process will ultimately depend on a range of energy constraints not presently considered.

4. Discussion

4.1. Crustal controls on MAFC processes

Factors that might control the extent of reaction of melt with the crust through which it migrates during ascent include the geometry of melt migration (i.e., whether in channels or along grain boundaries), the rate of melt supply and the melt–rock ratio at different levels in the crust. Evidence from oceanic gabbros suggests melt migration in the lower crust occurs as reactive porous flow through a crystal mush (e.g., Natland and Dick, 1996; Coogan et al., 2000; MacLeod and Yaouancq, 2000). Migration rate and the melt–rock ratio are dependent on the porosity and permeability of the mush (Hunter, 1996). The extent of reaction of melt with its surroundings might also be expected to depend on the amount of crust the melt passes through prior to eruption. Crustal thickness in the WVZ is generally in the range of 20–25 km (Bjarnason et al., 1993; Allen et al., 2002). Evidence for melt–wallrock interactions can be preserved in both the textures and compositions of gabbroic rocks as well as in the chemical signatures of erupted lavas, and crustal interaction has been called on to explain gabbro xenoliths from picritic lavas that show evidence for partial melting and mineral resorption (Larsen, 1979; Hansteen, 1991; Gurenko and Sobolev, 2006), and trace element and isotopic enrichments in Icelandic lavas (Muehlenbachs et al., 1974; Óskarsson et al., 1982; Condomines et al., 1983; Hémond et al., 1988; Nicholson et al., 1991, Maclennan, 2008b, Halldórsson et al., 2008a). Evidence from oceanic gabbro suites and ophiolites indicates melt–rock reaction may be a ubiquitous process in oceanic crust that is not unusually thick, and may be an important contributor to the geochemical evolution of MORB (Meyer et al., 1989; Natland and Dick, 1996; Coogan et al., 2000; Bédard et al., 2000; Kvassnes and Dick, 2000; Dick et al., 2002; Kvassnes, 2004; Kvassnes and Grove, 2008; Lissenberg and Dick, 2008).

Although a MAFC process involving wallrock assimilation successfully explains many of the chemical attributes of Lambahraun, the question remains as to where this assimilation is actually occurring. As higher pressures tend to favor clinopyroxene as a solid phase, increasing its stability field at the expense of olivine, it seems unlikely that this process can take place at great depth. Thermodynamic modeling of phase relations using MELTS (Ghiorso and Sack, 1995; Smith and Asimow, 2005) indicates clinopyroxene is likely to be on the solidus at pressures <4 kb for this basaltic melt composition. Under these conditions, olivine and plagioclase crystallization could occur simultaneously with partial melting of wallrock clinopyroxene provided heat transfer to the wallrock is sufficient to cause anatexis. As noted previously, the MAFC model is relatively insensitive to the melting mode, so we are unable to constrain the extent to which olivine and plagioclase may also be partially melted. Crystallization of olivine and plagioclase may effectively obscure any compositional contribution that melting of these phases might have, so while they may also be involved, the only distinguishable signature in the erupted basalts is the contribution from clinopyroxene.

One appealing attribute of the MAFC process is that it couples extent of fractionation and wallrock assimilation, with the most evolved (lowest MgO) rocks having the most crustal contamination. The spatial distribution (Fig. 4) observed in Lambahraun, in which lavas with higher incompatible elements tend to be located close to the vent while more distal lavas are less enriched, has also been observed in other Icelandic lava shields (Maclennan et al., 2003b; Sinton et al., 2005). However, this distribution also indicates a time dependency that is less intuitive: the last lavas erupted are also the most modified by a crustal contaminant. One possible explanation is that the eruption rate (melt extraction rate) decreases over time, so that the later lavas spend more time in the crust and thus have more time to evolve and interact with the surrounding wallrock. Additionally, the location of the assimilation process may change over time. Prolonged exposure to melt progressively heats up wallrock until it reaches its solidus temperature and starts melting. With a continuous but not necessarily constant melt flux, the location of the solidus migrates upwards through the crust over time so that later melts interact with wallrock higher in the transport column (Fig. 10). In this scenario, the latest melts would last equilibrate higher in the crust, with correspondingly lower temperature and lower MgO (e.g., Rubin and Sinton, 2007) than early melts that equilibrated at greater depths. The extent to which this scenario is reasonable will require careful consideration of the rates involved in the various processes, including heat exchange, melt velocity, mineral dissolution, and possibly diffusion.

Most existing evidence from oceanic gabbros indicates precipitation of clinopyroxene during melt–wallrock interaction, with dissolution of olivine and plagioclase (e.g., Meyer et al., 1989; Natland and Dick, 1996; Coogan et al., 2000; Kvassnes and Dick, 2000; Lissenberg and Dick, 2008), i.e., the opposite of the process we propose here. These studies examined the final stage in evolution of oceanic gabbros: the freezing of late-stage melts with precipitation of clinopyroxene, with or without simultaneous dissolution of olivine and plagioclase. However, when there has been a long time between eruptions and the crust has solidified, influx of magma into the system during new magmatic episodes might reverse this process, preferentially melting the wallrock clinopyroxene and precipitating magmatically-derived olivine ± plagioclase.

4.2. Lava shields and fissure eruptions in Iceland

Thjófahraun's geochemical variations and mineralogical progression with time are broadly consistent with evolution in a shallow magma chamber. Early lavas contain small amounts of olivine with little to no plagioclase. As the eruption continues over some months to years, the magma carries a greater proportion of plagioclase, consistent

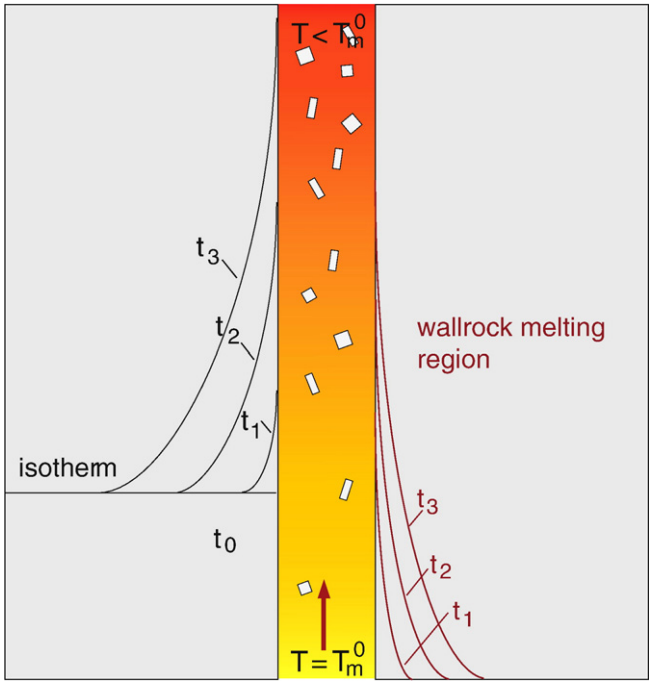

Fig. 10. Schematic representation of the MAFC process that couples extent of crustal assimilation and crystal fractionation during a period of continuous magma supply; t_1, t_2, t_3 represent progressively later times. Gray-shaded region is wallrock and the central, region is a schematic representation of a melt pathway with fractionating solids that is hotter at the base ($T = T_m^0$) than at the top ($T < T_m^0$). Lines on left side of melt pathway show evolution of a hypothetical isotherm; lines on right side show schematically how the wallrock solidus varies with time. With progressive supply of hot magma, the region of wallrock affected by partial melting expands upward and slightly outward with time. At later times, wallrock higher in the melt pathway will reach its solidus temperature. In this way, later lavas may have last equilibrated at lower magma temperatures and interacted with the most crust along its path.

with a single body of magma crystallizing at low pressure. The last lavas erupted are plagioclase-phyric 'a'ā flows with generally lower MgO (Fig. 5). Assuming this eruption taps a batch of resident magma, the minimum volume of reservoir melt is >1 km^3. Probably there was much more: estimates of the intrusive vs. extrusive volumes at Krafla in Iceland (Tryggvason, 1984, 1986; Sigurdsson, 1987), as well as geologic observations at Hess Deep (Stewart et al., 2005) and along the SEPR (Bergmanis et al., 2007), indicate less than half of the magma that exists in shallow magma chambers ever reaches the surface during rifting events. In simple models of a magma chamber filling and pressurizing prior to eruption, the erupted volume is a minimum constraint on the magma overpressure — that is, the amount of excess magma necessary to initiate diking to the surface — not the total volume of melt resident in the chamber. By some estimates, typical crustal reservoir volumes may be as high as 30 times the volume of erupted magma (Blake, 1981; Head et al., 1996). Once diking has reached the surface, magma can erupt fairly quickly, resulting in higher eruption rates, as indicated by lava morphology of the Thjófahraun flow field.

The nature of chemical heterogeneity in Lambahraun suggests that the erupted magmas may never have resided in a large, well-mixed magma chamber. Clinopyroxene barometry and major element chemistry indicates that some magma chambers in Iceland may be as deep as the lower crust or even upper mantle (Maclennan et al., 2001, 2003a, b). In the case of Lambahraun, if there is melt storage near the surface, it must be limited in extent and host little magma mixing. We envision crustal melt storage under Lambahraun as an interconnected network of many smaller melt bodies (pores to small melt lenses and sills), which primarily serve as pathways for melt migration rather than long-term storage (Fig. 11). In this scenario, the eruption rate may be dependent on the rates at which melt can be extracted from the mantle and migrate upwards through the crust. This is fundamentally different from a fissure eruption like Thjófahraun that is fed from a shallow chamber, in which the eruption proceeds relatively quickly once enough overpressure exists to initiate diking to the surface, erupting the excess magma and relieving the pressure in the chamber.

Although we have no direct evidence for a deep magma chamber beneath Lambahraun as has been posited for some other eruptive units in Iceland (Maclennan et al., 2001, 2003a,b), if there were melt storage near the crust–mantle boundary, an eruption from such a depth could result in a much greater volume of extrusive lava than from a shallow crustal reservoir. The overpressure required to reach the surface from near the crust–mantle boundary is greater, such that more eruptible magma must accumulate prior to diking in order to reach the surface and result in an eruption. Lava shield eruptions might begin as fissure-fed lava flows in the initial stages of the eruption when the driving pressure is high, gradually closing down to a few discrete centers of eruption, and eventually a single source vent (Rossi, 1996). It is this last stage in the eruption chronology, with its relatively low effusion rates but steady supply of magma that builds the classical lava shield morphology. This continued supply of magma through the crust and relatively low melt velocities could provide ideal conditions for melt–wallrock interaction.

Lambahraun is not the only post-glacial lava shield in the WVZ to show signs of crustal interaction. Although most other WVZ units are not as completely analyzed, a number of other shields exhibit the same geochemical signature of increasing CaO and incompatible element compositions with decreasing MgO, most notably Thingvallahraun, Hallmundarhaun and Leggjabrjótur (see Fig. 12; chemical data from Sinton et al., 2005). Although detailed study of the chemical and mineralogical variation in these units has not been undertaken, we consider them likely candidates for this process. All of these shields have large erupted volumes (6.3–10.8 km^3). Notably, we have not found the geochemical signature of crustal interaction in any of the fissure eruptions, although some lack sufficient data to fully describe geochemical evolution paths.

Icelandic fissure eruptions tend to occur with higher average effusion rates than the longer-lived shield eruptions, building rows of spatter cones and producing a higher proportion of 'a'ā units. It is possible that melt transport is too fast (or too short-lived) to heat the wallrock sufficiently to induce significant melting during fissure eruptions. In this scenario, crustal interaction might occur only in longer-lived, relatively low-effusion rate eruptive style of the large lava shields in the WVZ. However, because fissure eruptions are probably fed by moderate-sized crustal reservoirs, it is equally likely that any chemical signature of early crustal interaction was at least partially obscured during subsequent storage and mixing in shallow magma chambers. This hypothesis can explain some of the scatter in the Thjófahraun data, as incomplete or partial mixing may preserve some of the geochemical heterogeneity, which is then over-printed by the signature of subsequent crystallization in the magma chamber.

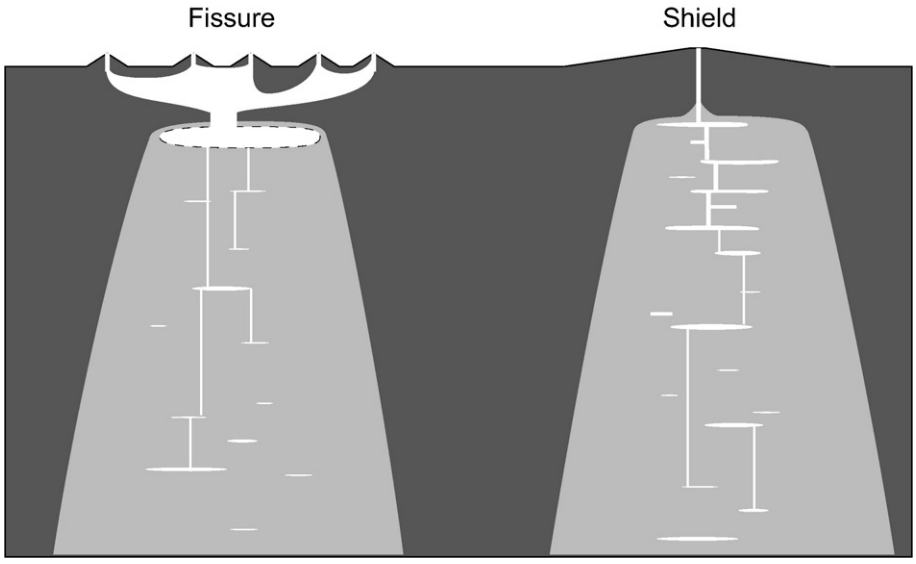

Fig. 11. Schematic representation of plumbing systems for Icelandic fissure and lava shield eruptions; sections drawn parallel to the rift zone axis. Evidence suggests that fissure eruptions are fed by shallow, moderately well-mixed magma chambers. In contrast, chemical variations in some lava shields are inconsistent with the presence of well-mixed reservoirs. Instead, we envision crustal melt storage under Lambahraun as an interconnected network of many smaller melt bodies (pores to small melt lenses and sills), which primarily serve as pathways for melt migration rather than long-term storage. Drawing not to scale.

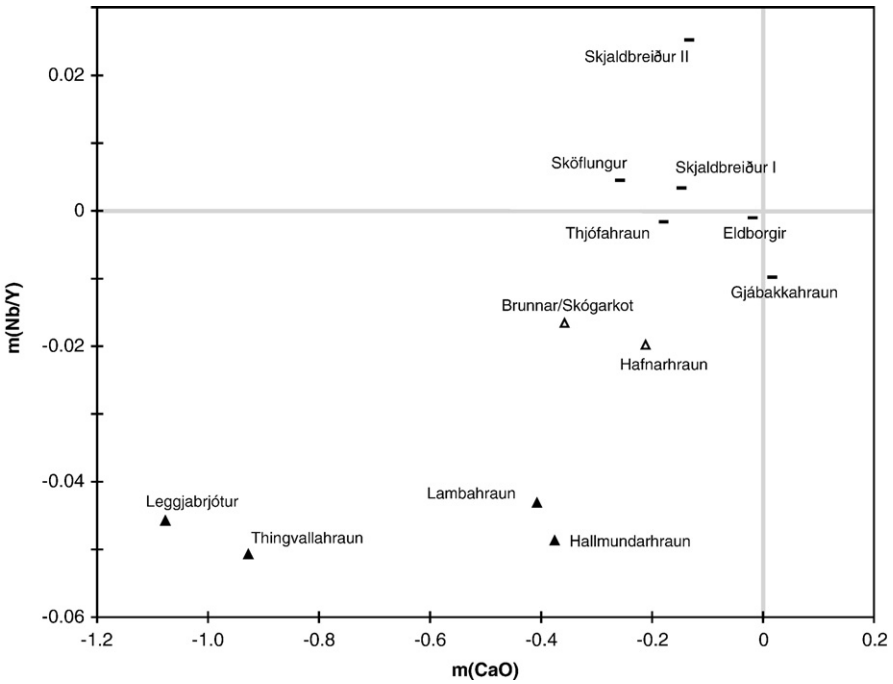

Fig. 12. *m*(Nb/Y) vs. *m*(CaO) for units in the Western Volcanic Zone with at least 10 whole-rock sample analyses, where *m* denotes the slope of regression lines plotted against the total range of MgO for each unit. Strongly negative slopes in Nb/Y (and other similar incompatible element ratios, not shown) vs. MgO generally correlate with steeper CaO vs. MgO variation for some large lava shields in the Western Volcanic Zone (solid triangles). These are the chemical signatures of the MAFC process identified for the Lambahraun lava shield. See text for discussion.

Taken together, our study supports the suggestion that Icelandic fissure eruptions represent short-lived, high-effusion eruptions that tap shallow melt reservoirs, while lava shields may lack shallow reservoirs and avoid the mixing that occurs in them.

Evidence suggests that crustal assimilation may be widespread in the Western Volcanic Zone, and could be more prevalent than the current data allow us to see. While the thick crust in Iceland might enhance crustal interaction processes, similar processes have been suggested to play a role in other mid-ocean ridge settings even where the crust is not unusually thick (Meyer et al., 1989; Natland and Dick, 1996; Coogan et al., 2000; Bédard et al., 2000; Kvassnes and Dick, 2000; Dick et al., 2002; Kvassnes, 2004; Kvassnes and Grove, 2008; Lissenberg and Dick, 2008) as well as at other hotspots (e.g., Pietruszka et al., 2009). We also emphasize that the process of crustal interaction can significantly alter major element concentrations and trace element ratios, parameters that are commonly used to infer melting conditions in many MORB studies. Although the MAFC process described in this paper is closely tied to the extent of differentiation as reflected in MgO contents, we also note that early crustal interaction and the chemical modifications it produces can be obscured by mixing in shallow magma chambers if shallow melt aggregation precedes eruption. These results suggest that inferences on melting conditions and source compositions may only be reliable for the least differentiated lava compositions from individual eruption sequences.

5. Conclusions

Thjófahraun and other fissure eruptions in Iceland represent short-lived, high effusion rate eruptions from an extant crustal reservoir. Early phases of Thjófahraun's eruption are dominated by olivine-phyric pāhoehoe lava with sample chemistry covering the full range of Thjófahraun's compositional variation, while later flow units transition to small-volume, plagioclase-phyric 'a'ā flows that tend to be more uniformly differentiated. Mineralogical and compositional variations are consistent with evolution in a shallow magma chamber.

The 7.3 km^3 Lambahraun lava shield is composed of dense pāhoehoe lava, indicating a relatively low effusion rate over a long-lived eruption. Spatial distribution of lava compositions suggests that the erupting magma became progressively more differentiated and enriched in incompatible elements with time during the eruption. Evidence for plagioclase accumulation is present in outcrops, thin section, and in the chemistry of some samples. Whole-rock compositional variations from Lambahraun are inconsistent with simple evolution in a shallow magma chamber, exhibiting increasing CaO and Nb/Zr with decreasing MgO content and incompatible element enrichments greater than predicted by crystal fractionation alone. The correlation of this enrichment with increasing differentiation and time during the eruption lead us to favor a process of concurrent wallrock assimilation and crystallization during melt migration through the crust, and we develop a MAFC model to explore the chemical effects of this process. The most evolved Lambahraun compositions are consistent with a total addition of 3–5% anatectic melt derived from less than 5% melting of the crust to the Lambahraun magmatic system. Similar geochemical characteristics exist in several other WVZ lava shields, but not in the available data from fissure eruptions. Crustal interaction might be more likely in long-lived, voluminous shield eruptions, where slow effusion could be related to low melt propagation velocities through thick crust.

Acknowledgements

We wish to thank Melissa Rotella and JoAnn Sinton for their assistance in the field and Karl Grönvold for his help and insight at many stages of this project, including extraordinary transportation services. Many thanks to Eric Hellebrand for his assistance with the microprobe and XRF analyses, Chuck Fraley for ICP-MS data collection, and JoAnn Sinton for the thin section preparation. We are also grateful to Rósa Ólafsdóttir for providing digitized topographic contours and a digital elevation model of the WVZ. This manuscript was greatly improved by thoughtful reviews by Laurence Coogan and John Maclennan. This

research was supported by National Science Foundation grant OCE05-24922. This is SOEST contribution 7793.

Appendix A. Supplementary data

Supplementary data associated with this article can be found, in the online version, at doi:10.1016/j.jvolgeores.2009.06.009.

References

Allen, R.M., Nolet, G., Morgan, W.J., Vogfjörd, K., Nettles, M., Ekström, G., Bergsson, B.H., Erlendsson, P., Foulger, G.R., Jakobsdóttir, S., Julian, B.R., Pritchard, M., Ragnarsson, S., Stefánsson, R., 2002. Plume-driven plumbing and crustal formation in Iceland. J. Geophys. Res. 107. doi:10.1029/2001JB000584.

Bédard, J.H., Hebert, R., Berclaz, A., Varfalvy, V., 2000. Syntexis and the genesis of lower oceanic crust. In: Dilek, Y., Moores, E.M., Elthon, D., Nicolas, A. (Eds.), Ophiolites and Oceanic Crust: New Insights from Field Studies and the Ocean Drilling Program: Special Paper, Geol. Soc. Am., vol. 349, pp. 105–119.

Bergmanis, E.C., Sinton, J., Rubin, K.H., 2007. Recent eruptive history and magma reservoir dynamics on the southern East Pacific Rise at 17°30′S. Geochem. Geophys. Geosyst. 8. doi:10.1029/2007GC001742.

Bjarnason, I.T., Menke, W., Flóvenz, Ó.G., 1993. Tomographic image of the mid-Atlantic plate boundary in southwest Iceland. J. Geophys. Res. 98, 6607–6622.

Björnsson, A., 1985. Dynamics of crustal rifting in NE Iceland. J. Geophys. Res. 90, 10151–10162.

Blake, S., 1981. Volcanism and the dynamics of open magma chambers. Nature 289, 783–785.

Chappell, B., 1992. Trace element analysis of rocks by X-ray spectrometry. Adv. X-ray Anal. 34, 263–276.

Condomines, M.K., Grönvold, K., Hooker, P.J., Muehlenbachs, K., O'Nions, R.K., Óskarsson, N., Oxburgh, E.R., 1983. He, O, Sr and Nd isotope relationships in Icelandic volcanics. Earth Planet. Sci. Lett. 66, 125–136.

Coogan, L.A., Saunders, A.D., Kempton, P.D., Norry, M.J., 2000. Evidence from oceanic gabbros for porous melt migration within a crystal mush beneath the Mid-Atlantic Ridge. Geochem. Geophys. Geosyst. 1. doi:10.1029/2000GC000072.

DePaolo, D.J., 1981. Trace element and isotopic effects of combined wallrock assimilation and fractional crystallization. Earth Planet. Sci. Lett. 53, 189–202.

Dick, H.J.B., Ozawa, K., Meyer, P.S., Niu, Y., Robinson, P.T., Constantin, M., Hebert, R., Maeda, J., Natland, J.H., Hirth, G., Mackie, S., 2002. Primary silicate mineral chemistry of a 1.5-km section of very slow spreading lower ocean crust: ODP Hole 735B, Southwest Indian Ridge. In: Natland, J.H., Dick, H.J.B., Miler, D.J., Von Herzen, R. (Eds.), Proceedings of the Ocean Drilling Program. Sci. Results, vol. 176. Ocean Drilling Program, College Station, TX, pp. 1–60.

Dunn, T., Sen, C., 1994. Mineral/matrix partition coefficients for orthopyroxene, plagioclase, and olivine in basaltic to andesitic systems: a combined analytical and experimental study. Geochim. Cosmochim. Acta 58, 717–734.

Embley, R.W., Chadwick, W.W., Perfit, M.R., Smith, M.C., Delaney, J.R., 2000. Recent eruptions on the CoAxial segment of the Juan de Fuca Ridge: implications for mid-ocean ridge accretion processes. J. Geophys. Res. 105, 16501–16526.

Ghiorso, M., Sack, R., 1995. Chemical mass-transfer in magmatic processes IV. A revised and internally consistent thermodynamic model for the interpolation and extrapolation of liquid–solid equilibria in magmatic systems at elevated temperatures and pressures. Contrib. Mineral. Petrol. 199, 197–212.

Green, T.H., 1994. Experimental studies of trace-element partitioning applicable to igneous petrogenesis: Sedona 16 years later. Chem. Geol. 117, 1–36.

Govindaraju, K., 1979. 1994 compilation of working values and sample descriptions for 383 geostandards. Geostand. Newsl. 18, 1–158.

Gurenko, A.A., Sobolev, A.V., 2006. Crust-primitive magma interaction beneath neovolcanic rift zone of Iceland recorded in gabbro xenoliths from Midfell, SW Iceland. Contrib. Mineral. Petrol. 151. doi:10.1007/S0041000600792.

Halldórsson, S.A., Óskarsson, N., Grönvold, K., Sigurdsson, G., Sverrisdóttir, G., Steinthorsson, S., 2008a. Isotopic-heterogeneity of the Thjorsa lava — implications for mantle sources and crustal processes within the Eastern Rift Zone, Iceland. Chem. Geol. 255. doi:10.1016/j.geochem.2008.06.050.

Halldórsson, S.A., Sinton, J., Grönvold, K., Sigurdsson, G., Sverrisdóttir, G., 2008b. Isotopic variations in postglacial volcanic products of the Western Rift Zone, Iceland. IAVCEI 2008 General Assembly, Reykjavík, Iceland: Abstract 1-b-P11.

Hansteen, T.H., 1991. Multi-stage evolution of the picritic Maelifell rocks, SW Iceland: constraints from mineralogy and inclusions of glass and fluid in olivine. Contrib. Mineral. Petrol. 109, 225–239.

Head, J.W.III, Wilson, L., Smith, D.K., 1996. Mid-ocean ridge eruptive vent morphology and substructure: evidence for dike widths, eruption rates, and evolution of eruptions and axial volcanic ridges. J. Geophys. Res. 101, 28265–28280.

Hémond, C., Condomines, M., Fourcade, S., Allègre, C.J., Óskarsson, N., Javoy, M., 1988. Th, Sr and O isotopic geochemistry in recent tholeiites from Iceland: crustal influence on mantle derived magmas. Earth Planet. Sci. Lett. 87, 273–285.

Hémond, C., Arndt, N.T., Lichtenstein, U., Hofmann, A.W., Óskarsson, N., Steinthorsson, S., 1993. The heterogeneous Iceland plume—Nd–S–O isotopes and trace-element constraints. J. Geophys. Res. 98, 15833–15850.

Howarth, R.J., 1998. Improved estimators of uncertainty in proportions, point-counting, and pass–fail test results. Am. J. Sci. 298, 594–607.

Hunter, R.H., 1996. Texture development in cumulate rocks. In: Cawthorn, R.G. (Ed.), Layered Intrusions. Elsevier, New York, pp. 77–101.

Jones, J.H., 1995. Experimental trace element partitioning. In: Ahrens, T.J. (Ed.), Rock Physics and Phase Relations: a Handbook of Physical Constants. AGU Reference Shelf, vol. 3. AGU, Washington, pp. 73–104.

Keleman, P.B., Yogodzinski, G.M., Scholl, D.W., 2003. Along-strike variation in the Aleutian Island Arc: genesis of high Mg# andesite and implications for continental crust. In: Eiler, J. (Ed.), Inside the Subduction Factory. AGU Monograph, vol. 138. AGU, Washington, pp. 223–246.

Kvassnes, A., 2004. The Evolution of Oceanic Gabbros: In-situ and Ancient Examples, Ph.D. Thesis, MIT, Woods Hole Joint Program in Oceanography.

Kvassnes, A., Dick, H.J., 2000. Deviations from dry fractionation trends in gabbros from Atlantis Bank, South West Indian Ocean. EOS. Trans. Am. Geophys. Union 82.

Kvassnes, A., Grove, T.L., 2008. How partial melts of mafic lower crust affect ascending magmas at oceanic ridges. Contrib. Mineral. Petrol. 156, 49–71.

LaFemina, P.C., Dixon, T.H., Malservisi, R., Arnadottir, T., Sturkell, E., Sigmundsson, F., Einarsson, P., 2005. Geodetic GPS measurements in south Iceland: Strain accumulation and partitioning in a propagating ridge system. J. Geophys. Res. 110. doi:10.1029/2005JB003675.

Larsen, J.G., 1979. Glass-bearing gabbro inclusions in hyaloclastites from Tindfjalljokull, Iceland. Lithos 12, 289–302.

Lissenberg, C.J., Dick, H.J.B., 2008. Melt–rock reaction in the lower oceanic crust and its implications for the genesis of mid-ocean ridge basalt. Earth Planet. Sci. Lett. 271, 311–325.

Maclennan, J., 2008a. Concurrent mixing and cooling of melts under Iceland. J. Petrol. 49, 1931–1953.

Maclennan, J., 2008b. Lead isotope variability in olivine-hosted melt inclusions from Iceland. Geochim. Cosmochim. Acta 72, 4159–4176.

Maclennan, J., McKenzie, D., Grönvold, K., Slater, L., 2001. Crustal accretion under northern Iceland. Earth Planet. Sci. Lett. 191, 295–310.

Maclennan, J., McKenzie, D., Grönvold, K., Shimizu, N., Eiler, J.M., Kitchen, N., 2003a. Melt mixing and crystallization under Theistareykir, northeast Iceland. Geochem. Geophys. Geosyst. 4. doi:10.1029/2003GC000558.

Maclennan, J., McKenzie, D., Hilton, F., Grönvold, K., Shimizu, N., 2003b. Geochemical variability in a single flow from northern Iceland. J. Geophys. Res. Lett. 108. doi:10.1029/2000JB000142.

MacLeod, C.J., Yaouancq, G., 2000. A fossil melt lens in the Oman ophiolite: implications for magma chamber processes at fast spreading ridges. Earth Planet. Sci. Lett. 176, 357–373.

McKenzie, D., O'Nions, R., 1991. Partial melt distributions from inversion of rare-earth element concentrations. J. Petrol. 32, 1021–1091.

McKenzie, D., O'Nions, R., 1995. The source regions of ocean island basalts. J. Petrol. 36, 133–159.

Metrich, N., Sigurdsson, H., Meyer, P.S., Devine, J.D., 1991. The 1783 Lakagigar eruption in Iceland: geochemistry, CO_2 and sulfur degassing. Contrib. Mineral. Petrol. 107, 435–447.

Meyer, P.S., Dick, H.J.B., Thompson, G., 1989. Cumulate gabbros from the Southwest Indian Ridge, 54°S–7°16′E: implications for magmatic processes at a slow spreading ridge. Contrib. Mineral. Petrol. 103, 44–63.

Moore, J.G., Calk, L.C., 1991. Degassing and differentiation in intraglacial volcanoes, Iceland. J. Volcanol. Geotherm. Res. 46, 157–180.

Muehlenbachs, K., Anderson, A.T., Sigvaldason, G.E., 1974. Low-^{18}O basalts from Iceland. Geochim. Cosmochim. Acta 38, 577–588.

Natland, J.H., Dick, H.J.B., 1996. Melt migration through high-level gabbroic cumulates of the East Pacific Rise at Hess Deep: the origin of magma lenses and the deep crustal structure of fast-spreading ridges. In: Mevel, C., Gillis, K.M., Allan, J.F., Meyer, P.S. (Eds.), Proceedings of the Ocean Drilling Program. Sci. Results, vol. 147. Ocean Drilling Program, College Station, TX, pp. 21–58.

Nichols, A.R.L., Carroll, M.R., Höskuldsson, Á., 2002. Is the Iceland hot spot also wet? Evidence from the water contents of undegassed submarine and subglacial pillow basalts. Earth Planet. Sci. Lett. 202, 77–87.

Nicholson, H., Condomines, M., Fitton, J.G., Fallick, A.E., Grönvold, K., Rogers, G., 1991. Geochemical and isotopic evidence for crustal assimilation beneath Krafla, Iceland. J. Petrol. 32, 1005–1020.

Norrish, K., Hutton, J., 1977. An accurate X-ray spectrographic method for the analysis of a wide range of geological samples. Geochim. Cosmochim. Acta 33, 431–441.

O'Hara, M.J., 1995. Trace element geochemical effects of integrated melt extraction and shaped melting regimes. J. Petrol. 34, 1111–1132.

O'Hara, M.J., 1998. Volcanic plumbing and the space problem — thermal and geochemical consequences of large-scale assimilation in ocean island development. J. Petrol. 39, 1077–1089.

Óskarsson, N., Sigvaldason, G.E., Steinthorsson, S., 1982. A dynamic model of the rift zone petrogenesis and the regional petrology of Iceland. J. Petrol. 23, 28–74.

Perfit, M.R., Chadwick Jr., W.W., 1998. Magmatism at mid-ocean ridges: constraints from volcanological and geochemical investigations. In: Buck, W.R., Delaney, P.T., Karson, J.A., Lagabrielle, Y. (Eds.), Faulting and Magmatism at Mid-Ocean Ridges, vol. 106. Amer. Geophy. Union Monogr., pp. 59–115.

Pietruszka, A.J., Hauri, E.H., Blichert-Toft, J., 2009. Crustal contamination of mantle-derived magmas within Piton de la Fournaise volcano, Reunion Island. J. Petrol. 50, 661–684.

Roeder, P.L., Emslie, R.F., 1970. Olivine-liquid equilibrium. Contrib. Mineral. Petrol. 29, 275–289.

Rossi, M.J., 1996. Morphology and mechanism of eruption of postglacial shield volcanoes in Iceland. Bull. Volcanol. 57, 530–540.

Rowland, S.K., Walker, G.P.L., 1990. Pahoehoe and aa in Hawaii: volumetric flow rate controls the lava structure. Bull. Volcanol. 52, 615–628.

Rubin, K.H., Sinton, J.M., 2007. Inferences on mid-ocean ridge thermal and magmatic structure from MORB compositions. Earth Planet. Sci. Lett. 260, 257–276.

Sæmundsson, K., 1991. Geology of the Krafla system. In: Gardarsson, A., Einarsson, A. (Eds.), Nattura Myvatns, Hid Islenska Natturufraedifelag, Reykjavik, pp. 25–95 (in Icelandic).
Sæmundsson, K., 1992. Geology of the Thingvallavatn area. Oikos 64, 40–68.
Schilling, J.-G., Zajac, M., Evans, R., Johnston, T., White, W., Devine, J.O., Kingsley, R., 1983. Petrologic and geochemical variations along the Mid-Atlantic Ridge from 29°N to 73°N. Am. J. Sci. 283, 510–586.
Shaw, D.M., 1970. Trace element fractionation during anatexis. Geochim. Cosmochim. Acta 34, 237–243.
Sigurdsson, H., 1987. Dyke injection in Iceland: a review. In: Halls, H.C., Fahrig, W.F. (Eds.), Mafic Dyke Swarms: Geol. Assoc. Can. Spec. Pap., vol. 34, pp. 55–64.
Sinton, J.M., Bergmanis, E., Rubin, K., Batiza, R., Gregg, T.K.P., Grönvold, K., Macdonald, K., White, S., 2002. Volcanic eruptions on mid-ocean ridges: new evidence from the superfast-spreading East Pacific Rise, 17°–19°S. J. Geophys. Res. 107. doi:10.1029/2000JB000090.
Sinton, J., Grönvold, K., Sæmundsson, K., 2005. Postglacial eruptive history of the Western Volcanic Zone, Iceland. Geochem. Geophys. Geosyst. 6. doi:10.1029/2005GC001021.
Smith, P., Asimow, P., 2005. Adiabat_1ph: a new public front-end to the MELTS, pMELTS, and pHMELTS models. Geochem. Geophys. Geosyst. 6. doi:10.1029/2004GC000816.
Spera, F., Bohrson, W., 2001. Energy-constrained open-system magmatic processes I: General model and energy-constrained assimilation and fractional crystallization (EC-AFC) formulation. J. Petrol. 42, 999–1018.
Stewart, M.A., Karson, J.A., Klein, E.M., 2005. Four-dimensional upper crustal construction at fast-spreading mid-ocean ridges: a perspective from an upper crustal cross-section at the Hess Deep Rift. J. Volcanol. Geotherm. Res. 144, 287–309.
Stracke, A., Zindler, A., Salters, J.M., McKenzie, D., Blichert-Toft, J., Albarède, F., Grönvold, K., 2003. Theistareykir revisited. Geochem. Geophys. Geosyst. 4. doi:10.1029/2001GC000201.
Sun, S.S., McDonough, W.F., 1989. Chemical and isotopic systematics of ocean island basalts: implications for mantle composition and processes. In: Saunders, A.D., Norry, M.J. (Eds.), Magmatism in the Ocean Basins: Geol. Soc. Spec. Publ., vol. 42, pp. 313–345.
Thirlwall, M.F., Gee, M.A.M., Taylor, R.N., Murton, B.J., 2004. Mantle components in Iceland and adjacent ridges investigated using double-spike Pb isotope ratios. Geochim. Cosmochim. Acta 68, 361–386.
Tryggvason, E., 1984. Widening of the Krafla fissure swarm during the 1975–1981 volcano-tectonic episode. Bull. Volcanol. 47, 47–69.
Tryggvason, E., 1986. Multiple magma reservoirs in a rift zone volcano: ground deformation and magma transport during the September eruption of Krafla, Iceland. J. Volcanol. Geotherm. Res. 28, 1–44.
Zindler, A., Hart, S.R., Frey, F.A., Jakobsson, S.P., 1979. Nd and Sr isotope ratios and Rare Earth Element abundances in Reykjanes Peninsula basalts: evidence for mantle heterogeneity beneath Iceland. Earth Planet. Sci. Lett. 45, 249–262.